The Multifaceted Role of EXOC6A in Ciliogenesis

Te-Lin Lin[1,2], Chien-Ting Wu[2,3], and Tang K. Tang[1,2,#]

1. Taiwan International Graduate Program in Molecular Medicine, National Yang Ming Chiao Tung University and Academia Sinica, Taipei, Taiwan
2. Institute of Biomedical Sciences, Academia Sinica, Taipei, Taiwan
3. Department of Microbiology, University of Texas Southwestern Medical Center, Texas, USA

Correspondence: Tang K. Tang, tktang@ibms.sinica.edu.tw

Abstract

Ciliogenesis is a highly ordered process that requires membrane trafficking, fusion, and maturation. In this study, we investigated EXOC6A, a component of the exocyst complex known for secretory vesicle trafficking and fusion, and found that it interacts with myosin-Va (Myo-Va) during ciliogenesis. EXOC6A colocalizes with Myo-Va at various stages of ciliogenesis, including preciliary vesicles, ciliary vesicles (CVs), and ciliary sheath membrane during ciliogenesis. We found that EXOC6A vesicles are actively recruited, integrated, and exit from the CVs and the ciliary sheath, implying that EXOC6A vesicles may facilitate continuous cilia membrane remodeling during ciliogenesis. Importantly, EXOC6A knockout impairs ciliogenesis, arresting most cells at the CV stage and preventing recruitment of NPHP and MKS module components to the transition zone. Furthermore, EXOC6A vesicles are transported to the mother centriole via a dynein-, microtubule-, and actin-dependent mechanism. Our results suggest that EXOC6A functions in both early and late stages of ciliogenesis and is involved in orchestrating vesicle dynamics, cilia membrane remodeling, and formation.

Keywords: Ciliogenesis, ciliary membrane assembly, intracellular pathway, exocyst complex, myosin-Va

Introduction

Most mammalian cells build primary cilia, which act as chemosensors or mechanosensors and as transducers that regulate key developmental signaling pathways. Primary cilia are composed of nine doublet microtubules arranged in a ring and surrounded by a ciliary membrane that is continuous with the plasma membrane (Dawe et al., 2007; Nigg and Raff, 2009). Primary cilia protrude from the cell surface to perform a wide range of biological functions. Defects in ciliogenesis can lead to a number of genetic disorders known as ciliopathies, which are characterized by loss of vision, disturbed kidney function, obesity, and defects in brain development (Sattar and Gleeson, 2011; Valente et al., 2014).

Ciliogenesis is a highly ordered and complex process. Currently, two distinct pathways have been reported, with different cell types involved: intracellular and extracellular. Polarized epithelial cells use the extracellular pathway, whereas fibroblasts and mesenchymal cells use the intracellular pathway (Breslow and Holland, 2019). In the intracellular pathway, myosin-Va (Myo-Va) facilitates the transportation of preciliary vesicles (PCVs) to the distal appendages (DAs) of the M-centrioles (Wu et al., 2018). These PCVs may be derived from the Golgi apparatus (Schmidt et al., 2012) and subsequently fuse with a ciliary vesicle (CV) through the action of membrane fusion regulators EHD1 and EHD3 (Lu et al., 2015).

This step is critical for the conversion of the mother centriole into a basal body, which is responsible for removing the centriole cap protein, CP110, and recruiting ciliary transition zone (TZ) proteins (Lu et al., 2015). As a result, an axoneme extends within the larger CV, which gradually stretches out to form the double membranes of the ciliary shaft and sheath that surround the extending axoneme. Finally, the ciliary sheath (the outer membrane) fuses with the plasma membrane and the axoneme, enveloped by the ciliary shaft membrane, extends from the cell membrane, and makes contact with the extracellular environment (Ghossoub et al., 2011). A signaling cascade including RAB11, RABIN8, and RAB8 has also been reported to regulate the ciliary membrane assembly (Chiba et al., 2013; Feng et al., 2012; Knödler et al., 2010; Nachury et al., 2007; Westlake et al., 2011; Yoshimura et al., 2007). However, the processes of formation of the ciliary sheath and ciliary shaft membrane during ciliogenesis remain unclear.

The exocyst is a multi-subunit protein complex that was first identified in yeast, which mediates the tethering of secretory vesicles to the plasma membrane (Mei and Guo, 2018). The complex is composed of eight subunits, named Sec (for secretion; Sec3, Sec5, Sec6, Sec8, Sec10, Sec15, Exo70, and Exo84) in yeast or Exoc (for exocyst-related; EXOC1 to 8) in humans (TerBush et al., 1996; TerBush and Novick, 1995).

The exocyst complex is implicated in various cellular processes, including exocytosis, ciliogenesis, cytokinesis, autophagy, cell polarity, migration, tumorigenesis, and fusion of secretory vesicles (Mei and Guo, 2018).

Mutations in genes encoding components of the exocyst complex have been associated with various human genetic disorders. For example, a mutation in *EXOC8* has been identified in Joubert syndrome (Dixon-Salazar et al., 2012), while a mutation in *EXOC4* has been reported in Meckel–Gruber syndrome (Shaheen et al., 2013). Both of these disorders involve clinically and genetically heterogeneous ciliopathy. Additionally, mutations in *EXOC2* cause severe defects in human brain development (Van Bergen et al., 2020), while mutations in *EXOC7* and *EXOC8* result in a novel disorder of cerebral cortex development, characterized by brain atrophy, seizures, developmental delay, and microcephaly (Coulter et al., 2020). However, the essential roles of these genes in ciliogenesis and their correlation with human genetic disorders are currently unknown.

It has been reported that some components of the exocyst complex are involved in ciliogenesis. For example, Sec10 (EXOC5) was shown to be required for ciliogenesis and cyst formation in vitro, and Sec10 knockdown leads to reduce ciliogenesis (Zuo et al., 2009; Zuo et al., 2019). Furthermore, other subunits such as EXOC3 and EXOC4 have been detected at the cilium with unknown function (Seixas et al., 2016). Interestingly, depletion of Sec8, Exo70, or Sec10 does not impair ciliogenesis (Rivera-Molina et al., 2021), whereas knockdown of Sec15a (EXOC6A) significantly perturbs ciliogenesis (Rivera-Molina et al., 2021). These findings imply that different exocyst subunits may have distinct, non-redundant functions during ciliogenesis. However, the precise localization of EXOC6A within cilia and its specific role in regulating ciliary membrane formation or trafficking events remain largely unknown.

Previously, we demonstrated that the earliest event in ciliogenesis is the transportation of PCVs by Myo-Va to the distal appendages of the M-centriole, and we showed that Myo-Va is released from the ciliary membrane upon fusion of the ciliary sheath with the plasma membrane (Wu et al., 2018). However, the mechanism of the assembly of double ciliary membranes (ciliary sheath and shaft) during intracellular ciliogenesis was left unknown. In this study, we provide evidence that the exocyst component EXOC6A interacts with Myo-Va and plays an essential role in ciliary membrane assembly at different stages during ciliogenesis.

Results

Colocalization patterns of EXOC6A and Myo-Va at preciliary vesicles, ciliary vesicles, and ciliary sheath during intracellular ciliogenesis

To investigate the localization of EXOC6A during ciliogenesis, we treated retinal pigment epithelial (RPE1)-based mCherry-tagged Myo-Va cargo binding domain (Myo-Va-GTD)-inducible cells with doxycycline (Dox) for 24 h and then serum starved them for 2h to induce ciliogenesis. We used antibodies against endogenous EXOC6A and glutamylated tubulin (Glu-tub), a marker of centrioles and ciliary axoneme, for confocal immunofluorescence analysis. Our results showed that the EXOC6A signal was mainly detected as a dot-shaped structure resembling a ciliary vesicle (CV) at the distal end of the M-centriole (Fig. 1A, left), while some EXOC6A signals appeared to be colocalized with mCherry-tagged Myo-Va-GTD at the ciliary membrane (Fig. 1A. right). To determine the subcellular localization of EXOC6A, we performed immunofluorescence staining using antibodies against CEP164 (a distal appendage marker, (Graser et al., 2007)) and CEP120 (a centriole marker, (Lin et al., 2013)). The PCV/CV/ciliary sheath can be visualized with mCherry-tagged Myo-Va-GTD (Wu et al., 2018). The cells were then analyzed using three-dimensional structured illumination microscopy (3D-SIM, Fig. 1B) or ultrastructure expansion microscopy (U-ExM, Fig. 1C). Our results showed that EXOC6A signals colocalized with mCherry-Myo-Va-GTD at CV (Fig. 1B and C). To further define the position of the EXOC6A signal, we performed correlative fluorescence light and electron microscopy (CFLEM) in RPE1-based GFP-EXOC6A-inducible cells (Fig. 1D). Our CFLEM results showed that the GFP-EXOC6A signals appeared to localize at PCVs (or vesicles), CVs (Fig. 1D-i-ii), and the elongating ciliary membrane (Fig. 1D-iii-iv).

To precisely analyze the subcellular localization of EXOC6A and Myo-Va during the formation of the ciliary sheath and the shaft membrane, we used 3D-SIM to analyze the RPE1 cells that exogenously express inducible GFP-EXOC6A using known markers combined for the ciliary sheath (Myo-Va-GTD; (Wu et al., 2018)), the ciliary shaft (ARL13B, INPP5E; (Feng et al., 2012; Garcia-Gonzalo et al., 2015; Wu et al., 2018), and the axoneme (Glu-tub). EXOC6A signals were commonly detected at the Myo-Va-GTD-labeled ciliary sheath (Fig. 1E-i, ii), which surrounds the ciliary shaft membrane (labeled ARL13B and INPP5E, Fig. 1E-i, iii) and the axoneme (Glu-tub, Fig. 1E-ii, iii). Since our 3D-SIM analysis could not distinguish the spatial distances between INPP5E and the Glu-tub-labeled axoneme due to the limits of its resolution power (100–130 nm), we thus conclude that EXOC6A localizes at the ciliary sheath membrane surrounding the ciliary shaft. Altogether, our data show that EXOC6A, like

Myo-Va, localizes at the PCVs, the CVs, and the ciliary sheath membrane.

Spatial and temporal localization of Myo-Va and EXOC6A during ciliogenesis

To investigate the temporal and spatial correlation between the ciliary localization of EXOC6A and Myo-Va during ciliogenesis, we used RPE1-based mCherry-Myo-Va-GTD-inducible cells that were serum starved, released at different time points, and analyzed using 3D-SIM with antibodies against endogenous EXOC6A and Glu-tub (Fig. 2A). We identified five different phenotypes based on the immunostaining patterns of Myo-Va and EXOC6A during cilium assembly (Fig. 2B), which are quantified in Fig. 2C. Before serum starvation, a number of EXOC6A-associated vesicles were detected close to the M-centriole (Fig. 2A, 0 min, type 1). During the progression of serum starvation, EXOC6A-associated vesicles appeared to gradually accumulate near the M-centriole (Fig. 2A, 15 min, type 2) in a process we called "clustering-to-centriole," and subsequently, EXOC6A signals were mainly detected at the Myo-Va-labeled CVs (Fig. 2A, 30 min–1 h, type 3) and the ciliary sheath membrane, surrounding the Glu-tub-labeled axoneme (Fig. 2A, 2 h, type 4). In some cells, a tubule-like structure ($EXOC6A^+$/$Myo\text{-}Va^+$) linked to the ciliary sheath membrane was observed (Fig. 2A, 4 h, white arrow). Finally, both EXOC6A and Myo-Va were released from the ciliary sheath membrane when it fused to the plasma membrane, while the Glu-tub-labeled axoneme continued to protrude into the extracellular milieu (Fig. 2A, 24 h, type 5). Interestingly, we observed that only a portion, but not all of the EXOC6A-labeled vesicles colocalized with Myo-Va-labeled PCVs (Fig. 2A, 0 and 15 min). However, once the CVs formed, both EXOC6A and Myo-Va-GTD signals were detected at the CVs (Fig. 2A, 30 min, 45 min, and 1 h). We present a schematic model in Figure 2B that shows the localization of EXOC6A (green) and mCherry-Myo-Va-GTD (red) during ciliogenesis and the types of immunostaining patterns.

To further understand the relationship between the clustering-to-centriole progression of EXOC6A and Myo-Va during the early stage of ciliogenesis, we analyzed the intensity of both proteins clustering to the centrioles and calculated their overlapping co-efficiency correlation R (Pearson correlation coefficient) using Zeiss Zen software (Fig. S1). We observed a gradual increase in the mean intensity of EXOC6A and Myo-Va clustering to the centrioles from 0 to 30 min (Fig. S1A–C). Additionally, the correlation R between EXOC6A and Myo-Va significantly increased from 0 to 30 min (Fig. S1D). These results suggest a high correlation between Myo-Va-labeled vesicles and EXOC6A-labeled vesicles during the progression of clustering-to-centriole.

FRAP analysis of the dynamic localization of Myo-Va- and EXOC6A-labeled

vesicles during ciliogenesis

We found that some EXOC6A labels had a tubule-like structure extending from the ciliary sheath (Fig. 2A, 4 h, type 4), suggesting the dynamic assembly of the ciliary membrane during ciliogenesis. To gain further insights into the dynamic relationship between Myo-Va- and EXOC6A-labeled vesicles during early CV formation and the later sheath membrane assembly stage, we performed live cell imaging with fluorescence recovery after photobleaching (FRAP). FRAP is a widely used technique to measure the dynamics of ciliary membrane protein localization (Kee et al., 2012; Westlake et al., 2011). After photobleaching at CVs or the ciliary sheath region, the EXOC6A signals were recurrently recruited to the CVs (Fig. 3A, Movie 1) and the ciliary sheath membrane immediately (Fig. 3B, Movie 2). Together, our data indicated that the EXOC6A-labeled vesicles are continuously recruited to and fused with the ciliary membrane not only at the CVs but also at the ciliary sheath. To further investigate the dynamic properties of the ciliary membrane, we performed live-cell super-resolution imaging using the ELYRA 7 SIM system. We used SiR-tubulin, a fluorescent probe derived from the microtubule-stabilizing drug docetaxel, to label endogenous microtubules. This allowed us to visualize the structure of centrioles and axonemes during ciliogenesis in live imaging experiments (Fig. S2). Our results show that EXOC6A co-localizes with Myo-Va-GTD on the ciliary membrane and surrounds the SiR-tubulin-labeled axoneme (Fig. S2A and S2B). In addition, we detected a dynamic tubule-like structure that extended and retracted from the ciliary membrane (Fig. S2A, S2C, and Movie 3). To better observe vesicle trafficking and membrane dynamics, we used the single-channel and burst modes of the ELYRA 7 SIM system to achieve higher temporal resolution in live imaging. Our results showed that GFP-EXOC6A-labeled vesicles gradually moved to and fused with CVs (Fig. 3C, white arrow; Movie 4) and the ciliary pocket, a membrane domain found at the base of primary cilia (Fig. 3D, white arrow, Movie 5). Interestingly, almost at the same time, some GFP-EXOC6A-labeled vesicles were fused with or secreted from the ciliary pocket (Fig. 3D, red arrow, Movie 5). Unexpectedly, we observed that some GFP-EXOC6A-associated tubular structures (Fig. 3D, yellow arrow) or GFP-EXOC6A-labeled vesicles were released directly from the ciliary membrane rather than from the ciliary pocket (Fig. 3D, orange arrow). Together, our results indicate that GFP-EXOC6A-associated vesicles/membranes are highly dynamic and continuously recruited to and/or released from CVs during the early stages of ciliogenesis, and that they are also fused with or excreted from the ciliary membrane during later stages of ciliogenesis. We, therefore, propose that EXOC6A vesicles are responsible for the exchange of materials within existing CVs and the ciliary sheath during ciliogenesis, facilitating the addition or removal of membranes or membrane proteins.

Myo-Va and EHD1 are required for EXOC6A-labeled CV formation, and EXOC6A is associated with Myo-Va

We previously reported that Myo-Va-mediated transportation of PCVs to the M-centriole is the earliest event that defines the onset of ciliogenesis (Wu et al., 2018). In this study, we aimed to examine the sequential order of PCV transportation mediated by Myo-Va and EXOC6A during ciliogenesis in both RPE1-based *Myo-Va* knockout (KO) and *EXOC6A* KO cells. Our results showed that few EXOC6A-labeled vesicles and no EXOC6A-labeled CVs were detected at the distal end of the M-centriole in the *Myo-Va* KO cells (Fig. 4A). In contrast, Myo-Va-labeled CVs were frequently observed at the M-centrioles of *EXOC6A* KO cells (Fig. 4B). Together, our findings suggest that EXOC6A is not essential for the formation of Myo-Va-labeled CVs during ciliogenesis.

EHD1 was reported to be essential for the fusion of PCVs to form larger CVs during the early stage of ciliogenesis (Lu et al., 2015). To investigate the sequential order of EHD1- and EXOC6A-mediated ciliary membrane assembly, we depleted EHD1 expression using siRNA in RPE1 cells. Our results showed that EHD1 depletion led to a reduction in the formation of EXOC6A-labeled CVs (Fig. 4C). In contrast, *EXOC6A* KO did not appear to affect EHD1-mediated fusion of PCVs to form a large EHD1-labeled CV at the M-centriole (Fig. 4D). Together, our findings suggest that EHD1 is required for EXOC6A-labeled CV formation, while EXOC6A is not essential for the formation of EHD1-labeled CVs

Additionally, previous studies reported that Myo2p, the yeast homolog of human Myo-Va, interacts with sec15, the yeast homolog of human EXOC6A (Jin et al., 2011). The present study showed that some, but not all of the EXOC6A-labeled PCVs colocalized with Myo-Va-labeled PCVs (Fig. 2A, 0 and 15 min). We speculate that Myo-Va may transport some EXOC6A-labeled vesicles to the CVs for ciliary membrane assembly. Our co-immunoprecipitation experiments showed that endogenous EXOC6A can co-immunoprecipitate with Myo-Va, supporting this hypothesis (Fig. 4E).

Finally, previous studies have indicated that the removal of centriolar protein CP110 from the distal end of the M-centriole is necessary for axoneme growth (Spektor et al., 2007). It has been proposed that CP110 removal occurs after the docking of CV to the DA of the M-centriole (Lu et al., 2015; Wu et al., 2018). To investigate the impact of EXOC6A loss on CP110 removal, we examined CP110 localization in *EXOC6A* KO cells. Our results showed that CP110 is appropriately removed from the distal end of the M-centriole in *EXOC6A* KO cells, indicating that EXOC6A is not required for this process (Fig. S3), which further support that EXOC6A is not essential for CV formation. Taken together, our findings suggest that Myo-Va transports a subset of EXOC6A-

labeled vesicles to the existing CVs of the M-centriole for ciliary membrane assembly. However, EXOC6A is not essential for CV formation.

Transportation of EXOC6A-labeled vesicles to the M-centriole is via a dynein-, MT-, and Arp2/3-dependent pathway

Our previous study showed that the transportation of PCVs to the distal appendages of the M-centriole is mediated by Myo-Va, dynein, microtubules (MTs), and the Arp2/3 complex (Wu et al., 2018). In the current study, we found that Myo-Va and EHD1 are required for EXOC6A-labeled CV formation and that Myo-Va co-immunoprecipitates with EXOC6A (Fig. 4). It has been reported that dynein is necessary for the correct positioning of the Golgi complex near the centrosome upon serum starvation (Palmer et al., 2009; Wu et al., 2018), and that the inhibition of dynein activity with ciliobrevin D suppresses ciliogenesis (Firestone et al., 2012; Wu et al., 2018). Therefore, we investigated whether the transport of EXOC6A-associated vesicles to the DA of the M-centriole also requires dynein, MTs, and the Arp2/3 complex.

RPE1 cells were transfected with siRNAs targeting Golgin160, a protein required for the recruitment of dynein to the Golgi complex (Yadav et al., 2012), or treated with ciliobrevin D, a known cytoplasmic motor dynein inhibitor that suppresses ciliogenesis (Firestone et al., 2012), following the protocol described in Figure 5A. Our findings showed that depletion of Golgin160 led to a decrease in EXOC6A-labeled CV signals at or near the M-centriole (Fig. 5B, D) and resulted in the dispersion of Golgi matrix protein 130 (GM-130)-labeled Golgi complexes (Fig. 5B, E), ultimately leading to a reduction in the total number of cilia (Fig. 5F). Similar results were also observed in RPE1 cells treated with ciliobrevin D (Fig. 5C-i, D–F). We next treated RPE1 cells with nocodazole (NZ, an MT-depolymerizing drug) and examined its effect on ciliogenesis. Our results showed that the EXOC6A-labeled CVs and the cilia number are greatly reduced in NZ-treated cells (Fig. 5C-ii, D, and F). These data suggest that some EXOC6A-labeled vesicles originate from Golgi, and the transportation of EXOC6A-associated vesicles to the M-centriole requires dynein and microtubules.

Since Myo-Va-mediated transport of PCVs to the M-centrioles relies on an Arp2/3-dependent branched actin network surrounding M-centrioles (Wu et al., 2018), we next treated RPE1 cells with siARP2 (Fig. 5G). A reduced cilia number (Fig. 5G and H) and reduced EXOC-6A-labeled CVs (Fig. 5G and I) were observed in siARP2-treated cells. A similar result was also found in cells treated with CK666 (a known specific Arp2/3 inhibitor) or high-dose (10 μM) cytochalasin D (CytoD), which has been reported to reduce the association of ARP2 with the branched actin network (Fig. 5H–J). It has been reported that low concentrations (100 nM-1 μM) of CytoD can promote

ciliogenesis and increase cilia length (Cao et al., 2023; Kim et al., 2015; Kim et al., 2010; Wu et al., 2018), while high concentrations (10 μm) lead to a significant inhibition of cilia formation (Wu et al., 2018). To further investigate the dose-dependent effects of actin cytoskeleton rearrangement on ciliogenesis, we treated RPE1 cells with CytoD at concentrations ranging from 200 nM to 10 μM. Immunofluorescence staining of cilia using ARL13B (green) and Glu-tubulin (red) antibodies showed that low concentrations of CytoD (200 nM–2 μM) resulted in significant cilia elongation, whereas higher doses (4 μM, 7μM and 10μM) gradually inhibited cilia formation (Fig. S4). Consistent with our previous findings (Wu et al., 2018), our data showed that cilia length and cilia ratio increased at low doses of CytoD (200 nM-2 μM) but gradually decreased with increasing doses (7 μM and 10 μM, Fig. S4B, S4C).

Taken together, our current studies reinforce our previous view (Wu et al., 2018) that low-dose of CytoD treatment (200 nM-2 μM) can stabilize and/or enhance the formation of Arp2-associated branched actin filaments. However when cells were treated with high doses of CytoD (7 μM and 10 μM, Fig. S4) or the specific Arp2/3 inhibitor, CK-666 (Fig. 5), the association of Arp2 with the branched actin network was significantly reduced, thereby inhibiting ciliogenesis. In conclusion, our data suggest that Myo-Va carries EXOC6A vesicles to the DA of mother centriole via a dynein-, microtubule-, and actin-dependent pathway.

Loss of EXOC6A inhibits ciliogenesis, and some cells exhibit abnormal ciliary morphology when passing through the CV block

We found that EXOC6A signals are detected at CVs and the ciliary sheath (Fig. 1 and 2). We also found that EXOC6A-associated vesicles are dynamically recruited to or excreted from CVs and/or the ciliary membrane (Fig. 3). We next examined the effects of *EXOC6A* deletion on ciliogenesis. As shown in Figure 6, *EXOC6A* KO significantly inhibits cilia assembly, resulting in either no cilia or dotted CV signals after serum starvation (SS, 30 min–48 h). Upon serum starvation for 30 min, Myo-Va-GTD-labeled CVs were detected at the M-centriole in both wild-type control and *EXOC*6A KO cells (Fig. 6A). In control cells, the Myo-Va-GTD signal was mainly detected at the ciliary sheath membrane (Fig. 6A, SS 2h) 2 h after serum starvation, while the Myo-Va-GTD signals dissociated from the ciliary sheath membrane after longer starvation (SS 24 h or SS 48 h). Interestingly, most Myo-Va-GTD signals in *EXOC6A* KO cells were present as dotted CVs after longer starvation (SS 48 h), suggesting that ciliogenesis is arrested at the CV stage (Fig. 6A, lower panel).

We next used an antibody against ARL13B (a cilia shaft marker) to label the ciliary membrane and found that most *EXOC6A* KO cells exhibited no cilia (~45%, Fig. 6C)

or dotted ARL13B signals (~50%) 2 h after SS (Fig. 6B; Fig. 6C, lower panel, SS 2 h), a pattern similar to Myo-Va staining (Fig. 6A, lower panel). Unexpectedly, after prolonged serum starvation, we could still detect approximately ~15% (SS 24 h) to ~30% (SS 48 h) of *EXOC6A* KO cells carrying ARL13B-labeled cilia protruding from the basal body. However, these ARL13B-labeled cilia showed a low intensity of ARL13B and Glu-tub signals (Fig. 6D and E) and the ARL13B-labeled cilia membrane exhibited a fragmented and punctuated staining pattern (enhanced in Fig. 6B, SS 48 h in lower panel). Our findings suggest that EXOC6A may play a crucial role in the further maturation of CVs into the ciliary sheath/shaft membrane during ciliogenesis.

To examine whether EXOC6A is required for ciliogenesis and whether its function can be rescued, we analyzed cilia formation in wild-type (WT), EXOC6A KO, and EXOC6A KO cells exogenously expressing GFP-EXOC6A. Immunofluorescence staining of cells with ARL13B and Glu-tubulin antibodies showed a significant reduction in the number of cilia in EXOC6A KO cells, while exogenous expression of GFP-EXOC6A in the KO cells can partially rescue cilia formation (Fig. S5).

Electron microscopy was further used to investigate the cilia morphology in the *EXOC6A* KO cells after prolonged serum starvation (72 h). To examine ciliary structure in *EXOC6A* KO cells in more detail, we used a 72 h-serum starvation protocol, which provided sufficient time for cilia assembly. Our results showed a perturbation in cilia assembly in *EXOC6A* KO cells (Fig. 6F and G). When compared with the wild-type control (Fig 6F-i and ii), cilia in *EXOC6A* KO cells exhibited some ciliogenic defects, such that ciliogenesis was often arrested at the DA/PCV or CV stage (Fig. 6F-iii and iv), and some exhibited morphologically curved cilia bending in the TZ region (Fig. 6F-vi, 4/37 in Fig. 6G). Intriguingly, a small proportion of KO cells produced an elongated large CV in the absence of an extended axoneme (Fig. 6F-v, 4/37 in Fig. 6G). Consistent with this finding, curved cilia (Fig. 6B, SS 24 h, lower panel) and a low intensity of Glu-tub-labeled axoneme were observed in *EXOC6A* KO cells via confocal immunofluorescence microscopy (Fig. 6B, SS 48 h, lower panel. Fig. 6E). Nonetheless, we still observed 3 out of 37 morphologically normal-like cilia in *EXOC6A* KO cells (Fig. 6F-vii, 6G). Taken together, our data suggest that depletion of EXOC6A primarily affects cells exhibiting no CV (showing only DA/PCV; Fig. 6F-iii, Fig. 6G) and/or arrests cells at the CV stage, while once it passes through CV stage after prolonged serum starvation, it may interfere with subsequent cilia membrane formation at later stages of ciliogenesis.

EXOC6A is required to recruit NPHP and MKS module components, but not

CEP290, to the TZ

Our EM study revealed both bending cilia at the TZ (4/37, Fig. 6G-vi) and morphologically normal-like cilia (3/37, Fig. 6G-vii). Intriguingly, immunofluorescence analysis revealed that the ARL13B signal intensity was greatly reduced in the normal-like cilia membrane in *EXOC6A* KO cells (Fig. 6D), suggesting a possible defect in the TZ of cilia. The TZ is a diffusion barrier at the ciliary membrane that acts as a gate to regulate the entry and exit of ciliary proteins required for signal transduction (Jensen and Leroux, 2017). Previous studies have identified three conserved protein modules (MKS, NPHP, and CEP290), composed of numerous protein complexes that cooperate in the assembly and gating function of the TZ (Gonçalves and Pelletier, 2017). CEP290, located at a proximal position near the M-centriole, acts as a hub that interacts with the NPHP and MKS module complexes (Garcia-Gonzalo and Reiter, 2017).

To verify the integrity of these abnormal cilia in *EXOC6A* KO cells, we examined the recruitment of several known TZ proteins, including CEP290, NPHP, and MKS module proteins. Our results showed that the recruitment of CEP290 to the ciliary base was normal in all examined ciliated cells, indicating that EXOC6A deletion did not affect CEP290 targeting to the TZ (Fig. 7A). However, the recruitment of several MKS complex proteins (TCTN2, AHI1, MKS3, and MKS1) to the basal body (M-centriole) was severely impaired in *EXOC6A* KO ciliated cells (Fig. 7B), while NPHP8 recruitment was only partially affected (Fig. 7B). Collectively, our findings suggest that EXOC6A is not required for CEP290 targeting to the TZ but plays an essential role in the recruitment of several NPHP and MKS module proteins to the basal body, which potentially affects the gating function of the TZ in *EXOC6A* KO cells.

Discussion

Cilia assembly is a complex, multistep process involving the accumulation and attachment of PCVs at the distal appendage, CV formation, and the subsequent extension of CVs into the ciliary sheath, alongside the formation of the ciliary shaft, ultimately leading to the mature cilia structure (Breslow and Holland, 2019; Long and Huang, 2019; Nachury et al., 2010). Currently, our understanding of the molecular mechanisms governing these steps remains incomplete. Exocytosis is a process where intracellular secretory vesicles fuse with the plasma membrane, aiding in delivering integral membrane proteins to the cell surface and releasing materials into the extracellular space (Martin-Urdiroz et al., 2016). Human EXOC6A exhibits a high degree of similarity to the product of the Saccharomyces cerevisiae *SEC15* gene. In yeast, SEC15 is essential for the movement of vesicles from the Golgi apparatus to the cell surface (Bowser and Novick, 1991). Previous studies have indicated that SEC15 interacts with Myo2p (the yeast homolog of human Myo-Va) and plays a role in vesicle exocytosis (Donovan and Bretscher, 2012; Donovan and Bretscher, 2015). Recently, exocyst was found to mediate the recycling of internal cilia and depletion of EXOC6A/Sec15a, but not other exocyst components, leads to a reduction in ciliogenesis (Rivera-Molina et al., 2021). This finding suggests that EXOC6A may have a unique function for ciliogenesis. However, the relationship and underlying mechanism between EXOC6A and Myo-Va in the context of ciliogenesis remain unclear.

In this study, we elucidated the role of the exocyst component EXOC6A in ciliogenesis and produced evidence for the model by which Myo-Va mediates trafficking of EXOC6A vesicles to the DA or existing CV of M-centriole in the early stages and to the ciliary membrane in the later stages of ciliogenesis (Figure 8). We found that a subset of EXOC6A-positive signals colocalized with Myo-Va-labeled signals during the early phase of ciliogenesis, and that they exhibited a high correlation during clustering-to-centriole progression after initiating ciliogenesis (Fig. S1A-D). Intriguingly, not all EXOC6A-labeled signals were positive for Myo-Va (Fig. 2A), suggesting the presence of at least two populations of Myo-Va-labeled vesicles in cells: one that is EXOC6A+/Myo-Va+ and another that is EXOC6A-/Myo-Va+ (Fig. 2A and Fig. 8).

In this model, ciliogenesis begins shortly after serum-starvation-induced quiescence. Initially, Myo-Va mediates the transport of PCVs (EXOC6A-/Myo-Va+ and EXOC6A+/Myo-Va+ vesicles) to the DA of the mother centriole, followed by the formation of PCVs to a CV via EHD1 (Lu et al., 2015; Wu et al., 2018). However, EXOC6A is not absolutely required for CV formation, as EXOC6A KO did not interfere

with the formation of Myo-Va- or EHD1-labelled CV (Fig. 4B, 4D). Once the CV is formed, the transport of EXOC6A vesicles to the existing CV in the early stages of ciliogenesis is still mediated by Myo-Va (Fig. 4A). The above process involves a two-step transportation mechanism: initially, dynein mediates the movement of Myo-Va-associated vesicles (either EXOC6A-positive or EXOC6A-negative) towards the pericentrosomal region along microtubules (MTs) (Fig. 5B–F). Subsequently, Myo-Va takes over and drives these vesicles (EXOC6A-positive or -negative) from the pericentrosomal region to the DAs of the M-centriole. This process is accomplished through the utilization of the ARP2/3-associated branched actin network (Fig. 5G–J). Notably, both of these Myo-Va-labeled vesicles require the function of EHD1 to form a CV (Fig. 4D; Wu et al., 2018). Our findings that EHD1 depletion (Fig. 4D) and *Myo-Va* KO (Fig. 4A) severely impaired the formation of EXOC6A-positive CVs at the M-centriole, suggest that Myo-Va and EHD1 play a role in promoting the formation of EXOC6-positive CVs during the early stages of ciliogenesis.

Although EXOC6A is not absolutely required for the initial CV formation (Fig. 4B, 4D), our data revealed another role of EXOC6A in the later stages of ciliogenesis. Our FRAP analysis and live cell imaging showed that a subset of EXOC6A-labeled vesicles displayed high dynamism throughout ciliogenesis, continually being recruited to, fusing into, or exited from existing CVs in the early stages and/or the ciliary membrane (or ciliary pocket) in the later stages of ciliogenesis (Fig. 3). These EXOC6A-positive vesicles, likely derived from the Golgi or recycling endocytic vesicles, are transported to the ciliary membrane (or ciliary pocket) and/or fused with/exited from the ciliary membrane in the later stages of ciliogenesis. The exocyst has been implicated in the transport of vesicles carrying ciliary proteins to the cilia (Wu and Guo, 2015). Thus, our findings suggested a potential role of EXOC6A vesicles, which may supply or remove proteins or lipid moieties from the CVs and/or the ciliary membrane (or ciliary pocket) during ciliogenesis.

Additionally, our results showed that *EXOC6A* KO led to the majority of the cells being arrested at the CV stage or exhibiting no or few cilia (Fig. 6C); only a small proportion of cilia were able to elongate, exhibiting an abnormal ciliary morphology (Fig. 6B, 6F). Electron microscopic analysis of these abnormal cilia revealed elongated CV (lacked axoneme, Fig. 6F-v,), curved cilia bending at the TZ region (Fig. 6F-vi), or normal-like cilia (Figure 6B-vii, whose structure and membrane composition need to be further characterized). Further confocal immunofluorescence analysis revealed a curved ciliary morphology (Fig. 6B, SS24h) and impaired recruitment of several known TZ proteins, including TCTN2, AHI1, MKS3, and MKS1, to the basal body in EXOC6A KO cells (Fig. 7). Taken together, our findings suggest that EXOC6A is required for the early and the later stages of ciliogenesis as providing or removing

ciliary components (proteins or membrane moieties) to the existing CV or ciliary membrane, which highlights its multifaceted involvement in the process of ciliary membrane formation.

Furthermore, the Rab11–Rabin8–Rab8 signaling pathway, which involves the recruitment of Rabin8 (a GDP–GTP exchange factor for Rab8) and subsequent activation of Rab8, has been implicated in ciliary membrane assembly (Knödler et al., 2010; Nachury et al., 2007; Westlake et al., 2011; Yoshimura et al., 2007). Recently, RAB34, located at the ciliary sheath (Ganga et al., 2021; Stuck et al., 2021), was also reported to be required for ciliogenesis (Xu et al., 2018). The relationship between EXOC6A, Rab11 signaling, and RAB34 in ciliogenesis is not clear. Future experiments dissecting the underlying mechanisms between Rab11 signaling, RAB34, and EXOC6A could provide a more complete picture of ciliary membrane assembly during ciliogenesis.

Finally, ciliopathy-associated genes have been demonstrated to impact various stages of mouse cortical development (Guo et al., 2015), and severe human ciliopathies are linked to developmental abnormalities in the forebrain (Andreu-Cervera et al., 2021). Mutations or deletions in genes encoding exocyst proteins, including *EXOC2*, *EXOC4*, *EXOC7*, and *EXOC8*, have been associated with ciliopathies and neural developmental disorders (Coulter et al., 2020; Dixon-Salazar et al., 2012; Shaheen et al., 2013; Turkyilmaz et al., 2021; Van Bergen et al., 2020). Interestingly, deletions involving the 5' portion of the *EXOC6A* gene and two adjacent cytochrome p450 genes (*CYP26A1* and *CYP26C1*) are associated with autosomal-dominant nonsyndromic optic aplasia (ONA), an extremely rare disorder that causes unilateral or bilateral blindness in the affected eye (Meire et al., 2011). The molecular basis remains unclear. Further studies are needed to explore the specific roles of various types of ciliary vesicles, the underlying mechanisms of their trafficking/fusion, and their relevance to ciliopathies and neural developmental disorders.

In summary, we have identified a novel role for EXOC6A in ciliogenesis and determined that it is essential for both early and late stages of this process. EXOC6A vesicles may transport proteins or lipid moieties to and from the CV (early phase) and the ciliary pocket/ciliary membrane (late phase) during ciliogenesis. However, EXOC6A is not absolutely necessary for the initial CV formation; its function may be to help assemble the complete transition zone and promote the maturation of existing CVs into the ciliary sheath/shaft membrane. Furthermore, transportation of EXOC6A vesicles to the mother centriole is mediated by Myo-Va and occurs via a dynein-, MT-, and Arp2/3-dependent pathway. Our study provides new insights into the function of EXOC6A in cilia membrane assembly during ciliogenesis. Future studies are needed to explore the specific roles of different types of ciliary vesicles, the underlying

mechanisms of their trafficking and fusion, and their relevance to ciliopathies and neural developmental disorders.

Methods

Plasmids and antibodies

cDNAs encoding full-length EXOC6A were obtained via RT–PCR using total RNAs from human HEK293T cells and subcloned in-frame into pcDNA4/TO/myc-His-A (Invitrogen) or pLVX-Tight-Puro (BD Biosciences Clontech) GFP expression vectors. GFP- and mCherry-myosin-Va-GTD constructs have been previously described (Wu et al., 2018). The sequences of all constructed plasmids were confirmed.

Commercial antibodies used were anti-Sec15 (clone [15S2G6], 1/100 for IF, Kerafast), anti-EXOC6 (1/100 for IF and 1/2000 for WB, Novus), anti-EXOC5 (1/2000 for WB, Proteintech), anti-EXOC7 (1/2000 for WB, Proteintech), anti-polyglutamylated tubulin (Glu-tub, GT335, 1/100 for IF, AdipoGen), anti-CEP164 (1/500 for IF, Novus), anti-GFP (Abcam and Clontech), anti-ARL13B (1/600 for IF, Proteintech), anti-myosin-Va (1/500 for IF and 1/5000 for WB, Novus), anti-EHD1 (1/500 for IF and 1/5000 for WB, Novus), anti-GM130 (1/1000 for IF, Abcam), anti-CP110 (1/600 for IF, Proteintech), anti-Golgin160 (1/2000 for WB, Novus), anti-Arp2 (1/1000 for WB, Abcam), anti-TMEM67 (MKS3, 1/400 for IF, Proteintech), anti-TCTN2 (1/400 for IF, Proteintech), anti-AHI1 (1/400 for IF, Proteintech), and anti-MKS1 (1/400 for IF, Proteintech). The secondary antibodies were Alexa 488/568/647 conjugated anti-mouse or rabbit (Invitrogen). The rabbit polyclonal antibody against CEP120 (residues 639–986) was as described in our previous paper (Lin et al., 2013; Tsai et al., 2019).

Cell culture and cell lines

Human telomerase-immortalized retinal pigment epithelial cells (RPE1) (Wu et al., 2018) originally obtained from ATCC were maintained in DMEM/F12 (1:1) supplemented with 10% FBS. Cells were transfected with various cDNA constructs using TransIT-LT1 Transfection Reagent (Mirus). All cell lines were tested for mycoplasma contamination and found negative.

The gRNA expression plasmids were obtained from Addgene (Addgene plasmid # 48138; http://n2t.net/addgene:48138 ; RRID:Addgene_48138), having been generated by inserting annealed primers into the gRNA cloning vector pSpCas9-2A-GFP (PX458) (Ran et al., 2013). The targeting sequences for the EXOC6A gRNA (gRNA1:5′-AAGTTACTGATACCAACCGA-3′ and gRNA2:5′- TTGTATCCGTAATCATGACA -

3′) primer pair purchased from Mission Biotech were annealed and cloned into PX458. For transfection, 2.5 μg gRNA (PX458 plasmid) was transfected with LT-1 reagent (Mirus) into RPE1 cells, according to the manufacturer's instructions. The transfected cells were sorted with GFP signals using a cell sorter (FACSAria, BD Biosciences) into single cells and expanded.

To confirm the depletion of EXOC6A, genomic DNAs isolated from *EXOC6A* knockout colonies were subjected to PCR using the following primers: 5′-TTGGGTCAGTGATTTGAATTG -3′ and 5′- CCAAATAATCTGTAATTCCCATA -3′ for gRNA1 and 5′- ACATCTCCTGAGCCTCATACC -3′ and 5′-GCTTCAGAAAAAGAGAATACTCCT -3′ for gRNA2. The sequences of PCR products were then confirmed. Also, the protein expression of expanded colonies was confirmed via IF and Western blotting.

RPE1-based doxycycline (DOX)-inducible cell lines were as described previously (Wu et al., 2018). To obtain RPE1 cell lines that inducibly expressed GFP-EXOC6A, GFP-Myo-Va-GTD, and mCherry-Myo-Va-GTD, lentiviruses generated using the target cDNAs in the pLVX-tight-puro vector were used to infect RPE1 Tet-On cells (stably expressing rtTA, Clontech). The infected cells were sterile-sorted using a cell sorter (FACSAria, BD Biosciences) for GFP or mCherry, and the positive cells were selected and expanded as inducible cell lines.

The siRNAs and non-targeting siRNA control were transfected into cells using Lipofectamine RNAiMAX (Invitrogen), according to the manufacturer's protocol. To increase knockdown efficiency, two rounds of silencing were used before the experiments. The siRNA sequences for siEHD1 (5′- GGAGAGAUCUACCAGAAGA-3′), siGolgin-160 (5′-CAGCCUCCUUGGCCGCGAGGGCCUC-3′), and siARP2 (5′-CCAGCUUUGGUUGGAAGACCUAUUA-3′) were purchased from Invitrogen.

Immunofluorescence confocal microscopy

Immunofluorescence confocal microscopy was carried out as previously described (Wu et al., 2018). Briefly, cells were grown on coverslips and fixed in methanol at −20 °C for 20 min. The cells were then blocked with 10% normal goat serum in PBST. After blocking, the cells were incubated with primary antibodies, washed with PBST, and then incubated with Alexa Fluor 488-, 568-, or 647-conjugated secondary antibodies (1/500; Invitrogen). The samples were visualized using an LSM880 Airyscan system (Carl Zeiss).

For the fluorescence recovery after photobleaching (FRAP) experiment, live imaging of RPE1-based GFP-EXOC6A and mCherry-myosin-Va-GTD cells was performed using the LSM880. A 405 nm laser was used to photobleach associated CVs and the ciliary sheath 100 times. The changes in fluorescence intensity of GFP-EXOC6A were measured from the projected z-stacks using ZEN software.

Super-resolution microscopy (3D-SIM)

The cells were fixed and stained as described (see above), and multi-colored beads (100 nm; Invitrogen) were added before mounting. Sixteen-bit super-resolution images with five phases and five rotations were obtained using a Zeiss ELYRA PS.1 LSM780 system or a Zeiss ELYRA7 system (Carl Zeiss). We used a plan-apochromatic 63×/1.4 NA oil-immersion M27 objective in combination with the default grid (stripe sim in ELYRA PS.1 and Lattice sim plus SIM square). We used the "optimized" setting for the z-stack interval. The raw images were reconstructed using ZEN Black (Carl Zeiss) under the default parameters. The reconstructed images were corrected with signals of beads for chromatic aberration in the *x*, *y*, and *z* directions, and the images were aligned accordingly with ZEN Black. We followed the standard guidelines (Demmerle et al., 2017) and used the SIM-Check software (Ball et al., 2015) to verify the raw, reconstructed, and calibrated data. To visualize centriole and axoneme structures during live-cell imaging, we employed SiR-tubulin, a fluorogenic probe that binds to endogenous microtubules (spirochrome).

Ultrastructure expansion microscopy (U-ExM)

U-ExM was used to reveal the fine cellular architecture of the cells. Cells were processed for this U-ExM as previously described (Gambarotto et al., 2019). In brief, cells were fixed with methanol or 4% PFA based on our target. First, cells on coverslips were incubated in a PBS solution containing 0.7% formaldehyde (FA; 36.5–38%; F8775; Sigma-Aldrich) plus 0.15% acrylamide (AA; 40%; A4058; Sigma-Aldrich) for 5 h at 37 °C. Next, the cells on coverslips were incubated in U-ExM monomer solution, composed of 19% (wt/wt) sodium acrylate (SA; 97–99%; 408220; Sigma-Aldrich), 10% (wt/wt) AA, and 0.1% (wt/wt) *N*,*N*′-methylenebisacrylamide (BIS; 2%; M1533; Sigma-Aldrich) at 37 °C for 1 h in the dark for gelation. We transferred coverslips with gel to 6-well plates, added 1 mL denaturing buffer (200 mM SDS, 200 mM NaCl, and 50 mM Tris in ultrapure water, pH 9), and shook for 15 min at room temperature (RT). We then separated gel from coverslips and transferred the gel to 1.5 mL centrifuge tubes with fresh denaturing buffer, then incubated at 95 °C for 30 min. After denaturation, the gels were placed in beakers filled with ddH2O overnight for expansion. For antibody staining, the gels were PBS washed and then incubated with primary antibodies for 1 or 2 nights at RT (depending on the antibodies). The gels were washed in PBST (PBS plus 0.1% tween20) and incubated with a secondary antibody for 3 h at 37 °C. The gels expanded by around 4x after this treatment. The samples were then visualized using an LSM880 Airyscan system (Carl Zeiss).

TEM and CFLEM

Cells were processed for transmission electron microscopy and CFLEM as previously described (Reddick and Alto, 2012). Briefly, RPE1 and RPE1-based *EXOC6A* KO cells were grown on Aclar film (Electron Microscopy Sciences) and fixed in 2% glutaraldehyde (GA) containing 1% tannic acid in 0.1 M cacodylate buffer. The fixed cells were post-fixed with 1% OsO_4 in 0.1 M cacodylate buffer at room temperature (RT) for 30 min. Then, the cells were further stained with 1% uranyl acetate at RT for 1 h, dehydrated in a graded series of ethanol, infiltrated, and embedded in Spurr's resin. Ultrathin sections (70 nm) were stained with 4% uranyl acetate (UA) and Reynold's lead citrate for 10 min and examined with an electron microscope (Tecnai G2 Spirit TWIN, FEI).

For CFLEM, RPE1-based GFP-EXOC6A-inducible cells were grown on laser-etched glass gridded coverslips affixed to the bottom of live-cell dishes (MatTek). Cells were treated with DOX for 24 h and serum starved for 2 or 24 h. The cells were then fixed with 2 % glutaraldehyde plus 1% tannic acid in 0.1 M cacodylate buffer, and the GFP-EXOC6A signals were imaged via 3D-SIM using a Zeiss ELYRA system (Carl Zeiss). The cells were then embedded in EPON resin. After EPON polymerization, resin blocks were detached from the glass dishes. Using the grid patterns imprinted in the resin, serial thin sections (70 nm) of the squares of interest were cut. The sections were stained with 4% uranyl acetate and Reynold's lead citrate for 10 min, and the cells were examined with an electron microscope (Tecnai G2 Spirit TWIN, FEI). All EM images were processed using Gatan Digital Micrograph software (Gatan).

Statistics and reproducibility

Statistical analyses were performed using GraphPad Prism. Results are presented as mean ± standard derivation (s.d.), as specified in the figure legends. Sample size and the number of repeated experiments are also described in the legends. Statistical differences between two datasets were analyzed using the two-tailed paired Student's *t*-test. The precise *P*-values are shown in the figures. $P < 0.05$ was considered statistically significant. All experiments were repeated at least three times.

Conflicts of interest

The authors declare no conflicts of interest.

Author contributions

Conceptualization: TLL and TKT; Investigation: TLL and CTW; Methodology: TLL, CTW, and TKT; Resource: TLL and TKT; Original Draft: TLL and TKT; Writing: TLL and TKT; Review & Editing: TLL, CTW, and TKT.

Acknowledgments

The authors acknowledge support from the Flow Cytometry Core Facility (IBMS, AS-CFII-111-212) for the cell-sorting service, the DNA Sequencing Core Facility (IBMS, AS-CFII-113-A12) for the DNA sequencing analysis, the Light Microscopy Core Facility (IBMS and IMB), and the EM core facilities (IMB and ICOB) of Academia Sinica. This work was supported by grants from Academia Sinica (AS-IA-109-L04) and the National Science and Technology Council, Taiwan (NSTC 112-2320-B-001-002; NSTC 112-2326-B-001-010) to TKT; and from the National Institutes of Health R01AI184984 to CTW.

References

Andreu-Cervera, A., M. Catala, and S. Schneider-Maunoury. 2021. Cilia, ciliopathies and hedgehog-related forebrain developmental disorders. *Neurobiol Dis*. 150:105236.

Ball, G., J. Demmerle, R. Kaufmann, I. Davis, I.M. Dobbie, and L. Schermelleh. 2015. SIMcheck: a Toolbox for Successful Super-resolution Structured Illumination Microscopy. *Sci Rep*. 5:15915.

Bowser, R., and P. Novick. 1991. Sec15 protein, an essential component of the exocytotic apparatus, is associated with the plasma membrane and with a soluble 19.5S particle. *The Journal of cell biology*. 112:1117-1131.

Breslow, D.K., and A.J. Holland. 2019. Mechanism and Regulation of Centriole and Cilium Biogenesis. *Annual review of biochemistry*. 88:691-724.

Cao, M., X. Zou, C. Li, Z. Lin, N. Wang, Z. Zou, Y. Ye, J. Seemann, B. Levine, Z. Tang, and Q. Zhong. 2023. An actin filament branching surveillance system regulates cell cycle progression, cytokinesis and primary ciliogenesis. *Nature Communications*. 14:1687.

Chiba, S., Y. Amagai, Y. Homma, M. Fukuda, and K. Mizuno. 2013. NDR2-mediated Rabin8 phosphorylation is crucial for ciliogenesis by switching binding

specificity from phosphatidylserine to Sec15. *The EMBO journal*. 32:874-885.
Coulter, M.E., D. Musaev, E.M. DeGennaro, X. Zhang, K. Henke, K.N. James, R.S. Smith, R.S. Hill, J.N. Partlow, A.-S. Muna, A.S. Kamumbu, N. Hatem, A.J. Barkovich, J. Aziza, N. Chassaing, M.S. Zaki, T. Sultan, L. Burglen, A. Rajab, L. Al-Gazali, G.H. Mochida, M.P. Harris, J.G. Gleeson, and C.A. Walsh. 2020. Regulation of human cerebral cortical development by EXOC7 and EXOC8, components of the exocyst complex, and roles in neural progenitor cell proliferation and survival. *Genetics in Medicine*. 22:1040-1050.
Dawe, H.R., H. Farr, and K. Gull. 2007. Centriole/basal body morphogenesis and migration during ciliogenesis in animal cells. *Journal of cell science*. 120:7-15.
Demmerle, J., C. Innocent, A.J. North, G. Ball, M. Müller, E. Miron, A. Matsuda, I.M. Dobbie, Y. Markaki, and L. Schermelleh. 2017. Strategic and practical guidelines for successful structured illumination microscopy. *Nat Protoc*. 12:988-1010.
Dixon-Salazar, T.J., J.L. Silhavy, N. Udpa, J. Schroth, S. Bielas, A.E. Schaffer, J. Olvera, V. Bafna, M.S. Zaki, G.H. Abdel-Salam, L.A. Mansour, L. Selim, S. Abdel-Hadi, N. Marzouki, T. Ben-Omran, N.A. Al-Saana, F.M. Sonmez, F. Celep, M. Azam, K.J. Hill, A. Collazo, A.G. Fenstermaker, G. Novarino, N. Akizu, K.V. Garimella, C. Sougnez, C. Russ, S.B. Gabriel, and J.G. Gleeson. 2012. Exome sequencing can improve diagnosis and alter patient management. *Sci Transl Med*. 4:138ra178.
Donovan, K.W., and A. Bretscher. 2012. Myosin-V is activated by binding secretory cargo and released in coordination with Rab/exocyst function. *Dev Cell*. 23:769-781.
Donovan, K.W., and A. Bretscher. 2015. Tracking individual secretory vesicles during exocytosis reveals an ordered and regulated process. *The Journal of cell biology*. 210:181-189.
Feng, S., A. Knodler, J. Ren, J. Zhang, X. Zhang, Y. Hong, S. Huang, J. Peranen, and W. Guo. 2012. A Rab8 guanine nucleotide exchange factor-effector interaction network regulates primary ciliogenesis. *The Journal of biological chemistry*. 287:15602-15609.
Firestone, A.J., J.S. Weinger, M. Maldonado, K. Barlan, L.D. Langston, M. O'Donnell, V.I. Gelfand, T.M. Kapoor, and J.K. Chen. 2012. Small-molecule inhibitors of the AAA+ ATPase motor cytoplasmic dynein. *Nature*. 484:125-129.
Gambarotto, D., F.U. Zwettler, M. Le Guennec, M. Schmidt-Cernohorska, D. Fortun, S. Borgers, J. Heine, J.-G. Schloetel, M. Reuss, M. Unser, E.S. Boyden, M. Sauer, V. Hamel, and P. Guichard. 2019. Imaging cellular ultrastructures using expansion microscopy (U-ExM). *Nature Methods*. 16:71-74.
Ganga, A.K., M.C. Kennedy, M.E. Oguchi, S. Gray, K.E. Oliver, T.A. Knight, E.M. De La Cruz, Y. Homma, M. Fukuda, and D.K. Breslow. 2021. Rab34 GTPase mediates

714 ciliary membrane formation in the intracellular ciliogenesis pathway. *Curr Biol*.
715 31:2895-2905.e2897.
716 Garcia-Gonzalo, F.R., S.C. Phua, E.C. Roberson, G. Garcia, 3rd, M. Abedin, S. Schurmans,
717 T. Inoue, and J.F. Reiter. 2015. Phosphoinositides Regulate Ciliary Protein
718 Trafficking to Modulate Hedgehog Signaling. *Dev Cell*. 34:400-409.
719 Garcia-Gonzalo, F.R., and J.F. Reiter. 2017. Open Sesame: How Transition Fibers and the
720 Transition Zone Control Ciliary Composition. *Cold Spring Harb Perspect Biol*. 9.
721 Ghossoub, R., A. Molla-Herman, P. Bastin, and A. Benmerah. 2011. The ciliary pocket:
722 a once-forgotten membrane domain at the base of cilia. *Biology of the cell*.
723 103:131-144.
724 Gonçalves, J., and L. Pelletier. 2017. The Ciliary Transition Zone: Finding the Pieces and
725 Assembling the Gate. *Mol Cells*. 40:243-253.
726 Graser, S., Y.D. Stierhof, S.B. Lavoie, O.S. Gassner, S. Lamla, M. Le Clech, and E.A. Nigg.
727 2007. Cep164, a novel centriole appendage protein required for primary cilium
728 formation. *The Journal of cell biology*. 179:321-330.
729 Guo, J., H. Higginbotham, J. Li, J. Nichols, J. Hirt, V. Ghukasyan, and E.S. Anton. 2015.
730 Developmental disruptions underlying brain abnormalities in ciliopathies. *Nat*
731 *Commun*. 6:7857.
732 Jensen, V.L., and M.R. Leroux. 2017. Gates for soluble and membrane proteins, and
733 two trafficking systems (IFT and LIFT), establish a dynamic ciliary signaling
734 compartment. *Curr Opin Cell Biol*. 47:83-91.
735 Jin, Y., A. Sultana, P. Gandhi, E. Franklin, S. Hamamoto, A.R. Khan, M. Munson, R.
736 Schekman, and L.S. Weisman. 2011. Myosin V transports secretory vesicles via
737 a Rab GTPase cascade and interaction with the exocyst complex. *Dev Cell*.
738 21:1156-1170.
739 Kee, H.L., J.F. Dishinger, T.L. Blasius, C.J. Liu, B. Margolis, and K.J. Verhey. 2012. A size-
740 exclusion permeability barrier and nucleoporins characterize a ciliary pore
741 complex that regulates transport into cilia. *Nat Cell Biol*. 14:431-437.
742 Kim, J., H. Jo, H. Hong, M.H. Kim, J.M. Kim, J.K. Lee, W.D. Heo, and J. Kim. 2015. Actin
743 remodelling factors control ciliogenesis by regulating YAP/TAZ activity and
744 vesicle trafficking. *Nat Commun*. 6:6781.
745 Kim, J., J.E. Lee, S. Heynen-Genel, E. Suyama, K. Ono, K. Lee, T. Ideker, P. Aza-Blanc, and
746 J.G. Gleeson. 2010. Functional genomic screen for modulators of ciliogenesis
747 and cilium length. *Nature*. 464:1048-1051.
748 Knödler, A., S. Feng, J. Zhang, X. Zhang, A. Das, J. Peränen, and W. Guo. 2010.
749 Coordination of Rab8 and Rab11 in primary ciliogenesis. *Proc Natl Acad Sci U S*
750 *A*. 107:6346-6351.
751 Lin, Y.N., C.T. Wu, Y.C. Lin, W.B. Hsu, C.J. Tang, C.W. Chang, and T.K. Tang. 2013. CEP120

interacts with CPAP and positively regulates centriole elongation. *J Cell Biol*. 202:211-219.

Long, H., and K. Huang. 2019. Transport of Ciliary Membrane Proteins. *Front Cell Dev Biol*. 7:381.

Lu, Q., C. Insinna, C. Ott, J. Stauffer, P.A. Pintado, J. Rahajeng, U. Baxa, V. Walia, A. Cuenca, Y.S. Hwang, I.O. Daar, S. Lopes, J. Lippincott-Schwartz, P.K. Jackson, S. Caplan, and C.J. Westlake. 2015. Early steps in primary cilium assembly require EHD1/EHD3-dependent ciliary vesicle formation. *Nat Cell Biol*. 17:228-240.

Martin-Urdiroz, M., M.J. Deeks, C.G. Horton, H.R. Dawe, and I. Jourdain. 2016. The Exocyst Complex in Health and Disease. *Frontiers in Cell and Developmental Biology*. 4.

Mei, K., and W. Guo. 2018. The exocyst complex. *Current Biology*. 28:R922-R925.

Meire, F., I. Delpierre, C. Brachet, F. Roulez, C. Van Nechel, F. Depasse, C. Christophe, B. Menten, and E. De Baere. 2011. Nonsyndromic bilateral and unilateral optic nerve aplasia: first familial occurrence and potential implication of CYP26A1 and CYP26C1 genes. *Mol Vis*. 17:2072-2079.

Nachury, M.V., A.V. Loktev, Q. Zhang, C.J. Westlake, J. Peranen, A. Merdes, D.C. Slusarski, R.H. Scheller, J.F. Bazan, V.C. Sheffield, and P.K. Jackson. 2007. A core complex of BBS proteins cooperates with the GTPase Rab8 to promote ciliary membrane biogenesis. *Cell*. 129:1201-1213.

Nachury, M.V., E.S. Seeley, and H. Jin. 2010. Trafficking to the ciliary membrane: how to get across the periciliary diffusion barrier? *Annu Rev Cell Dev Biol*. 26:59-87.

Nigg, E.A., and J.W. Raff. 2009. Centrioles, centrosomes, and cilia in health and disease. *Cell*. 139:663-678.

Palmer, K.J., H. Hughes, and D.J. Stephens. 2009. Specificity of cytoplasmic dynein subunits in discrete membrane-trafficking steps. *Mol Biol Cell*. 20:2885-2899.

Ran, F.A., P.D. Hsu, J. Wright, V. Agarwala, D.A. Scott, and F. Zhang. 2013. Genome engineering using the CRISPR-Cas9 system. *Nat Protoc*. 8:2281-2308.

Reddick, L.E., and N.M. Alto. 2012. Correlative light and electron microscopy (CLEM) as a tool to visualize microinjected molecules and their eukaryotic sub-cellular targets. *J Vis Exp*:e3650.

Rivera-Molina, F.E., Z. Xi, E. Reales, B. Wang, and D. Toomre. 2021. Exocyst complex mediates recycling of internal cilia. *Current Biology*. 31:5580-5589.e5585.

Sattar, S., and J.G. Gleeson. 2011. The ciliopathies in neuronal development: a clinical approach to investigation of Joubert syndrome and Joubert syndrome-related disorders. *Developmental medicine and child neurology*. 53:793-798.

Schmidt, K.N., S. Kuhns, A. Neuner, B. Hub, H. Zentgraf, and G. Pereira. 2012. Cep164 mediates vesicular docking to the mother centriole during early steps of

ciliogenesis. *The Journal of cell biology*. 199:1083-1101.

Seixas, C., S.Y. Choi, N. Polgar, N.L. Umberger, M.P. East, X. Zuo, H. Moreiras, R. Ghossoub, A. Benmerah, R.A. Kahn, B. Fogelgren, T. Caspary, J.H. Lipschutz, and D.C. Barral. 2016. Arl13b and the exocyst interact synergistically in ciliogenesis. *Mol Biol Cell*. 27:308-320.

Shaheen, R., E. Faqeih, M.J. Alshammari, A. Swaid, L. Al-Gazali, E. Mardawi, S. Ansari, S. Sogaty, M.Z. Seidahmed, M.I. AlMotairi, C. Farra, W. Kurdi, S. Al-Rasheed, and F.S. Alkuraya. 2013. Genomic analysis of Meckel–Gruber syndrome in Arabs reveals marked genetic heterogeneity and novel candidate genes. *European Journal of Human Genetics*. 21:762-768.

Spektor, A., W.Y. Tsang, D. Khoo, and B.D. Dynlacht. 2007. Cep97 and CP110 suppress a cilia assembly program. *Cell*. 130:678-690.

Stuck, M.W., W.M. Chong, J.C. Liao, and G.J. Pazour. 2021. Rab34 is necessary for early stages of intracellular ciliogenesis. *Curr Biol*. 31:2887-2894.e2884.

TerBush, D.R., T. Maurice, D. Roth, and P. Novick. 1996. The Exocyst is a multiprotein complex required for exocytosis in Saccharomyces cerevisiae. *The EMBO journal*. 15:6483-6494.

TerBush, D.R., and P. Novick. 1995. Sec6, Sec8, and Sec15 are components of a multisubunit complex which localizes to small bud tips in Saccharomyces cerevisiae. *The Journal of cell biology*. 130:299-312.

Tsai, J.-J., W.-B. Hsu, J.-H. Liu, C.-W. Chang, and T.K. Tang. 2019. CEP120 interacts with C2CD3 and Talpid3 and is required for centriole appendage assembly and ciliogenesis. *Scientific Reports*. 9:6037.

Turkyilmaz, A., E. Kurnaz, and A. Cayir. 2021. First Report of a de novo 10q23.31q23.33 Microdeletion: Obesity, Intellectual Disability and Microcephaly. *Mol Syndromol*. 12:258-262.

Valente, E.M., R.O. Rosti, E. Gibbs, and J.G. Gleeson. 2014. Primary cilia in neurodevelopmental disorders. *Nature reviews. Neurology*. 10:27-36.

Van Bergen, N.J., S.M. Ahmed, F. Collins, M. Cowley, A. Vetro, R.C. Dale, D.H. Hock, C. de Caestecker, M. Menezes, S. Massey, G. Ho, T. Pisano, S. Glover, J. Gusman, D.A. Stroud, M. Dinger, R. Guerrini, I.G. Macara, and J. Christodoulou. 2020. Mutations in the exocyst component EXOC2 cause severe defects in human brain development. *J Exp Med*. 217.

Westlake, C.J., L.M. Baye, M.V. Nachury, K.J. Wright, K.E. Ervin, L. Phu, C. Chalouni, J.S. Beck, D.S. Kirkpatrick, D.C. Slusarski, V.C. Sheffield, R.H. Scheller, and P.K. Jackson. 2011. Primary cilia membrane assembly is initiated by Rab11 and transport protein particle II (TRAPPII) complex-dependent trafficking of Rabin8 to the centrosome. *Proc Natl Acad Sci U S A*. 108:2759-2764.

Wu, B., and W. Guo. 2015. The Exocyst at a Glance. *Journal of cell science*. 128:2957-2964.

Wu, C.T., H.Y. Chen, and T.K. Tang. 2018. Myosin-Va is required for preciliary vesicle transportation to the mother centriole during ciliogenesis. *Nat Cell Biol*. 20:175-185.

Xu, S., Y. Liu, Q. Meng, and B. Wang. 2018. Rab34 small GTPase is required for Hedgehog signaling and an early step of ciliary vesicle formation in mouse. *Journal of cell science*. 131.

Yadav, S., M.A. Puthenveedu, and A.D. Linstedt. 2012. Golgin160 recruits the dynein motor to position the Golgi apparatus. *Dev Cell*. 23:153-165.

Yoshimura, S., J. Egerer, E. Fuchs, A.K. Haas, and F.A. Barr. 2007. Functional dissection of Rab GTPases involved in primary cilium formation. *The Journal of cell biology*. 178:363-369.

Zuo, X., W. Guo, and J.H. Lipschutz. 2009. The exocyst protein Sec10 is necessary for primary ciliogenesis and cystogenesis in vitro. *Mol Biol Cell*. 20:2522-2529.

Zuo, X., G. Lobo, D. Fulmer, L. Guo, Y. Dang, Y. Su, D.V. Ilatovskaya, D. Nihalani, B. Rohrer, S.C. Body, R.A. Norris, and J.H. Lipschutz. 2019. The exocyst acting through the primary cilium is necessary for renal ciliogenesis, cystogenesis, and tubulogenesis. *The Journal of biological chemistry*. 294:6710-6718.

Figure Legends

Figure 1. Colocalization patterns of EXOC6A and myosin-Va at preciliary vesicles, ciliary vesicles, and ciliary sheath during ciliogenesis.

(A) RPE1-based mCherry-Myo-Va-GTD cells were treated with Dox for 24 h, followed by serum starvation for 2h. Cells were then stained with antibodies against EXOC6A (green) and polyglutamylated tubulin (Glu-tub) (gray) and analyzed using immunofluorescence confocal microscopy. (B and C) RPE1-based mCherry-Myo-Va-GTD-inducible cells were treated as described in A and immunostained with antibodies against EXOC6A (green), CEP120 (centriole marker), and CEP164 (distal appendage marker, gray). Images were captured using 3D-SIM or ultra-expansion microscopy (U-ExM) with an LSM880 confocal system. (D) CFLEM analysis of the localization of GFP-EXOC6A during ciliogenesis. RPE1-based GFP-EXOC6A-inducible cells were treated with Dox for 24 h and subjected to serum starvation for 2 or 24 h to observe the CVs or cilia membrane, respectively. Images were taken via SIM and TEM and then merged based on their relative localization. GFP-EXOC6A signals were located at PCVs, CVs (i-ii), and the ciliary membrane (iii-iv). (E) RPE1-based GFP-EXOC6A and mCherry-Myo-Va-GTD-inducible cells were treated with Dox for 24 h and analyzed via 3D-SIM using the indicated antibodies. Right panels show fluorescence profile plots. EXOC6A colocalized with myosin-Va at the ciliary sheath, while ARL13B (i) and INPP5E (iii) are the ciliary shaft markers. Scale bars are 1 μm.

Figure 2. Spatial–temporal localization of EXOC6A and Myo-Va during ciliogenesis.

(A) RPE1-based mCherry-Myo-Va-GTD-inducible cells were treated with Dox for 24 h, serum starved, released at different time points, and analyzed via 3D-SIM using the indicated antibodies. The white arrow indicates a tubule extending from the ciliary membrane. (B, C) Schematic model showing the localization patterns of EXOC6A (green) and Myo-Va (red) during ciliogenesis, and the percentages of cells with different types of staining patterns (%) are shown in C. Scale bars are 1 μm.

Figure 3. FRAP analysis of Myo-Va- and EXOC6A-labeled vesicles during ciliogenesis.

(A and B) RPE1-based GFP-EXOC6A and mCherry-Myo-Va-GTD-inducible cells were treated with Dox for 24 h and serum starved for 30 min. Regions of CVs (A) or

the ciliary membrane (B) of the cells were photobleached using the LSM880 confocal microscope with the 405 nm laser (related to Movies 1 and 2). Signal intensity of EXOC6A is shown in the right panel. (C and D) Dynamic localization of GFP-EXOC6A at CVs (C) or the ciliary membrane (D) during ciliogenesis. RPE1-based GFP-EXOC6A-inducible cells were treated with Dox for 24 h and serum starved for 30 min. Images were taken using an Elyra 7 high-speed live-cell imaging system. Series of images in (C) shows the progression of fusion of GFP-EXOC6A-associated vesicles into CVs (white arrow). Series of images in (D) shows the process by which GFP-EXOC6A-associated vesicles fuse into the ciliary pocket (white arrow) and simultaneously exit or reintegrate into the ciliary pocket (red arrow). Some images also show the release of tubule-like structures in the ciliary membrane (yellow arrow), or the excretion of vesicles in the ciliary membrane (orange arrow). These data suggested that the components of CVs, the ciliary pocket, and the ciliary membrane are highly dynamic (related to Movies 4 and 5). Scale bars are 2 μm.

Figure 4. Myo-Va and EHD1 are required for EXOC6A-labeled CV formation, and EXOC6A is associated with Myo-Va.

(A) Myo-Va is required for EXOC6A-labeled CV formation. RPE1-based *Myo-Va* KO cells and WT cells immunostained with antibodies against EXOC6A (green) and Glu-tub (red). Quantification of cells with EXOC6A-positive CVs (middle panel) and immunoblotting results (right panel) are shown. (B) EXOC6A is not required for Myo-Va-labeled CV formation. RPE1-based mCherry-Myo-Va-GTD-inducible cells against *EXOC6A* KO background and WT cells were immunostained with antibodies against Glu-tub (red). For easy differentiation, the mCherry-Myo-Va-GTD signal is converted to green. Quantification of cells with Myo-Va-associated CVs (middle panel) and immunoblotting results (right panel) are shown. (C) EHD1 is required for EXOC6A-labeled CV formation. RPE1 cells treated with siControl or siEHD1 for 48 h were immunostained with antibodies against EXOC6A (green) and Glu-tub (red). Quantification of cells with EXOC6A-positive CVs (middle panel) and immunoblotting results (right panel) are shown. (D) EXOC6A is not required for EHD1-labeled CV formation. RPE1-based *EXOC6A* KO and WT cells were immunostained with antibodies against EHD1 (green) and Glu-tub (red). Quantification of cells with EHD1-positive CVS is shown (right panel). (E) Co-IP experiments analyzed the association between EXOC6A and its potential binding proteins. Cell lysates were immunoprecipitated (IP) with EXOC6A or Myo-Va antibodies, followed by immunoblotting with the indicated antibodies. Error bars in A–D represent mean ± s.d. from at least 3 independent experiments with 100 cells per experiment. P-value was

921 determined with two-tailed Student's t-test. $P < 0.05$ was considered statistically
922 significant. NS, not significant. Scale bars are 1 μm.
923

924 **Figure 5. Transportation of EXOC6A-associated vesicles to the M-centriole occurs**
925 **via a dynein-, actin-, and MT-dependent pathway**

926 (A) Schematic showing the protocols of siRNA (left) or drug (right) treatment. (B)
927 RPE1 cells were treated with siControl or siGolgin160 and analyzed via confocal
928 fluorescence microscopy or immunoblotting using the indicated antibodies. (C) RPE1
929 cells were treated with ciliobrevin D (i) or nocodazole (ii) and analyzed via confocal
930 fluorescence microscopy using the indicated antibodies. (D-F) Cells with EXOC6A-
931 associated CVs (D), a positioned Golgi (E), or a cilia ratio (F) were analyzed via 3D-
932 SIM and quantified. Cells with a positioned Golgi were defined as those showing all
933 GM130-labeled Golgi signals concentrated within a 7 μm radius surrounding the Glu-
934 tub-labeled centrioles. (G) RPE1-based mCherry-myosin-Va-GTD-inducible cells were
935 treated with siARP2 as described in A (left) and analyzed via confocal microscopy or
936 immunoblotting using the indicated antibodies. (H, I) Quantifications of the cilia ratio
937 (H) and EXOC6A-associated CVs (I) is shown. (J) RPE1 cells were treated with CK666
938 or high-dose (10 μM) CytoD as described in A (right panel) and analyzed via confocal
939 microscopy using the indicated antibodies. Quantification of the cilia ratio (H) and
940 EXOC6A-associated CVs (I) is shown. * in (B, right panel) indicates non-specific
941 bands. Error bars represent mean ± s.d. from at least 3 independent experiments with
942 100 randomly selected cells. P-value was determined with two-tailed Student's t-test.
943 $P < 0.05$ was considered statistically significant. NS, not significant. Scale bars are 1
944 μm.

945 **Figure 6. Loss of EXOC6A inhibits ciliogenesis, and some cells exhibit an**
946 **abnormal ciliary morphology when passing through the CV block.**

947 (A-C) RPE1-based mCherry-Myo-Va-GTD-inducible WT and *EXOC6A* KO cells
948 were treated with Dox for 24 h, serum starved (SS) at different time points, and
949 analyzed via confocal fluorescence microscopy with the indicated antibodies. mCherry-
950 Myo-Va-GTD signal is artificially converted to green for discrimination. (B) RPE1 WT
951 and *EXOC6A* KO cells were serum starved at different time points and analyzed via
952 confocal fluorescence microscopy with the indicated antibodies. For comparison, the
953 intensities of ARBL13B and Glu-tub of *EXOC6A* KO cells with non-enhanced and
954 enhanced signals are shown in B (lower panel). (C) Cilia ratio measured through
955 ARL13B labeling (non-enhanced signal). (D and E) Quantitation of non-enhanced
956 ARL13B (D) and non-enhanced Glu-tub intensity on cilia (E) of WT or EXOC6A KO

cells is shown. (F) WT and *EXOC6A* KO cells were serum starved for 72 h. Morphologies of normal or abnormal cilia, including DA, CVs, and ciliary membranes, were examined via EM (F) and quantified (G; N is the number of cells examined). Error bars in C, D, and E represent mean ± s.d. from at least 3 independent experiments from 100 randomly selected cells. P-value was determined with two-tailed Student's t-test. $P < 0.05$ was considered statistically significant. NS, not significant. Scale bars are 1 μm in A and B. Scale bars are 500 nm in F.

Figure 7. EXOC6A is required for the recruitment of MKS module proteins to the peripheral TZ.

(A) WT and *EXOC6A* KO cells were fixed for 2 h (A) or 24 h (B) after serum starvation and analyzed via confocal fluorescence microscopy using antibodies against TZ proteins. Glu-tub staining labeled the centriole. Quantification of the fluorescence signals of various MKS proteins and NPHP8 on ciliated WT or EXOC6A KO cells is shown in the right panel. Error bars represent the mean ± s.d. from at least 3 independent experiments with 100 randomly selected cells per experiment. P-value was determined with two-tailed Student's t-test. $P < 0.05$ was considered statistically significant. NS, not significant. Scale bars, 1 μm.

Figure 8. Ciliogenesis model and comparison between WT and *EXOC6A* KO cells.

EXOC6A is located at the PCV/CV/ciliary sheath, and Myo-Va mediated the transportation of EXOC6A vesicles to the mother centriole via a dynein-, microtubule-, and actin-dependent pathway. EXOC6A-associated vesicles are continuously recruited and fused or excreted from the CVs or ciliary membrane. Depletion of EXOC6A impairs ciliogenesis, and most cells are arrested at the CV stage. There is a lack of MKS module proteins of the TZ in cilia with defects in *EXOC6A* KO cells. PCV, preciliary vesicle; CV, ciliary vesicle; DA, distal appendage; sDA, subdistal appendage.

Supplementary Figure 1. Correlation of spatial localization of EXOC6A and Myo-Va during the early stages of ciliogenesis.

(A) RPE1-based mCherry-Myo-Va-GTD-inducible cells were treated with DOX for 24 h and serum starved for 0, 15, and 30 min. Fluorescence intensities of EXOC6A (green) or Myo-Va-GTD (red) signals within a 2 μm radius surrounding the Glu-tub-labeled centrioles (white) were quantified and are shown in B (EXOC6A) and C (Myo-Va-GTD). Correlation R (Pearson correlation coefficient) between EXOC6A and Myo-Va is shown in D. Correlation R was analyzed using Zeiss Zen blue software. Error bars in

B–D represent mean ± s.d. from at least 3 independent experiments with 100 randomly selected cells. P-value was determined with one-way ANOVA. $P < 0.05$ was considered statistically significant. NS, not significant. Scale bars are 1 μm.

Supplementary Figure 2. Live-cell imaging of GFP-EXOC6A co-localized with Myo-Va-GTD at the ciliary membrane

(A) RPE1-based inducible cells expressing GFP-EXOC6A and mCherry-MyoVa-GTD were treated with Dox for 24 h, serum starved for 30 min, and SiR-tubulin was added to label centriole and axoneme. (B) Single channel image (green box in A) captured at the starting time point (0 sec). (C) Single channel image (red box in A) captured at frame 21 (197.577 sec). Scale bars are 1 μm.

Supplementary Figure 3. *EXOC6A* deletion does not interfere with the removal of CP110 from the mother centriole.

WT and *EXOC6A* KO cells were fixed 24 h after serum starvation and analyzed via fluorescence confocal microscopy using the indicated antibodies. (B) Percentages of cells with one or two CP110 dots are shown. Error bars represent the mean ± s.d. from at least 3 independent experiments with 100 cells per experiment. P-value was determined with two-tailed Student's t-test. NS, not significant. Scale bars are 1 μm.

Supplementary Figure 4. Low doses of Cytochalasin D (CytoD) promote cilia elongation, whereas higher concentrations (greater than 4 μM) inhibit ciliogenesis.

(A) RPE1 cells were treated with different concentrations of Cytochalasin D (CytoD), including control (0.1% DMSO), 200 nM, 1 μM, 2 μM, 4 μM, 7 μM, and 10 μM. Quantification of ciliary length labeled with ARL13B antibody (B) and cilia ratio (C) are shown. P-values were determined with a two-tailed Student's t-test. $P < 0.05$ was considered statistically significant. Error bars represent the mean ± s.d. of 100 randomly selected cells from at least 3 independent experiments. Scale bars are 2 μm.

Supplementary Figure 5. Rescue of ciliogenesis defects in EXOC6A knockout cells by GFP-EXOC6A re-expression.

(A) Representative immunofluorescence images of RPE1 cells (WT, WT+GFP-EXOC6A, *EXOC6A* KO, and *EXOC6A* KO+GFP-EXOC6A) stained for ARL13B (red) and Glu-tubulin (white). **(B)** Quantitative analysis of ARL13B-labeled cilia phenotypes. Data are presented as the mean ± s.d. of 100 randomly selected cells from at least three

independent experiments. Scale bars are 1 μm.

Source Data. Uncropped images of Western blots shown in the main figures.

Supplementary Video

Supplementary Video 1 Related to Fig. 3A. RPE1-based inducible cells expressing GFP-EXOC6A and mCherry-Myo-Va-GTD were treated with Dox for 24 h and then serum starved for 30 min. Live cell images were taken using an LSM880 Carl Zeiss confocal system under a controlled CO2 (5%) and temperature (37 °C). Photobleaching was performed on the CVs. The first time point of photobleaching the CVs was at 2 min, following which the CVs gradually recovered.

Supplementary Video 2 Related to Fig. 3B. RPE1-based inducible cells expressing GFP-EXOC6A and mCherry-Myo-Va-GTD were treated with Dox for 24 h and then serum starved for 30 min. Live cell images were taken using an LSM880 Carl Zeiss confocal system under a controlled CO2 (5%) and temperature (37 °C). Photobleaching was performed on the ciliary membrane. The first photobleaching time point for the ciliary membrane was at 2 min, after which the ciliary membrane gradually recovered.

Supplementary Video 3 Related to Fig. S2. RPE1-based inducible cells expressing GFP-EXOC6A and mCherry-MyoVa-GTD were treated with Dox for 24 h, then serum starved for 30 min, and SiR-tubulin was added to label centriole and axoneme. Live cell images were acquired using an Elyra 7 SIM Carl Zeiss confocal system under a controlled CO2 (5%) and temperature (37 °C).

Supplementary Video 4 Related to Fig. 3C. RPE1-based inducible cells expressing GFP-EXOC6A were treated with Dox for 24 h and then serum starved for 30 min. Live cell images were taken using an Elyra 7 SIM Carl Zeiss confocal system under a controlled CO2 (5%) and temperature (37 °C).

Supplementary Video 5 Related to Fig. 3D. RPE1-based inducible cells expressing GFP-EXOC6A were treated with Dox for 24 h and then serum starved for 30 min. Live cell images were taken using an Elyra 7 SIM Carl Zeiss confocal system under a controlled CO2 (5%) and temperature (37 °C).

Figure. 1

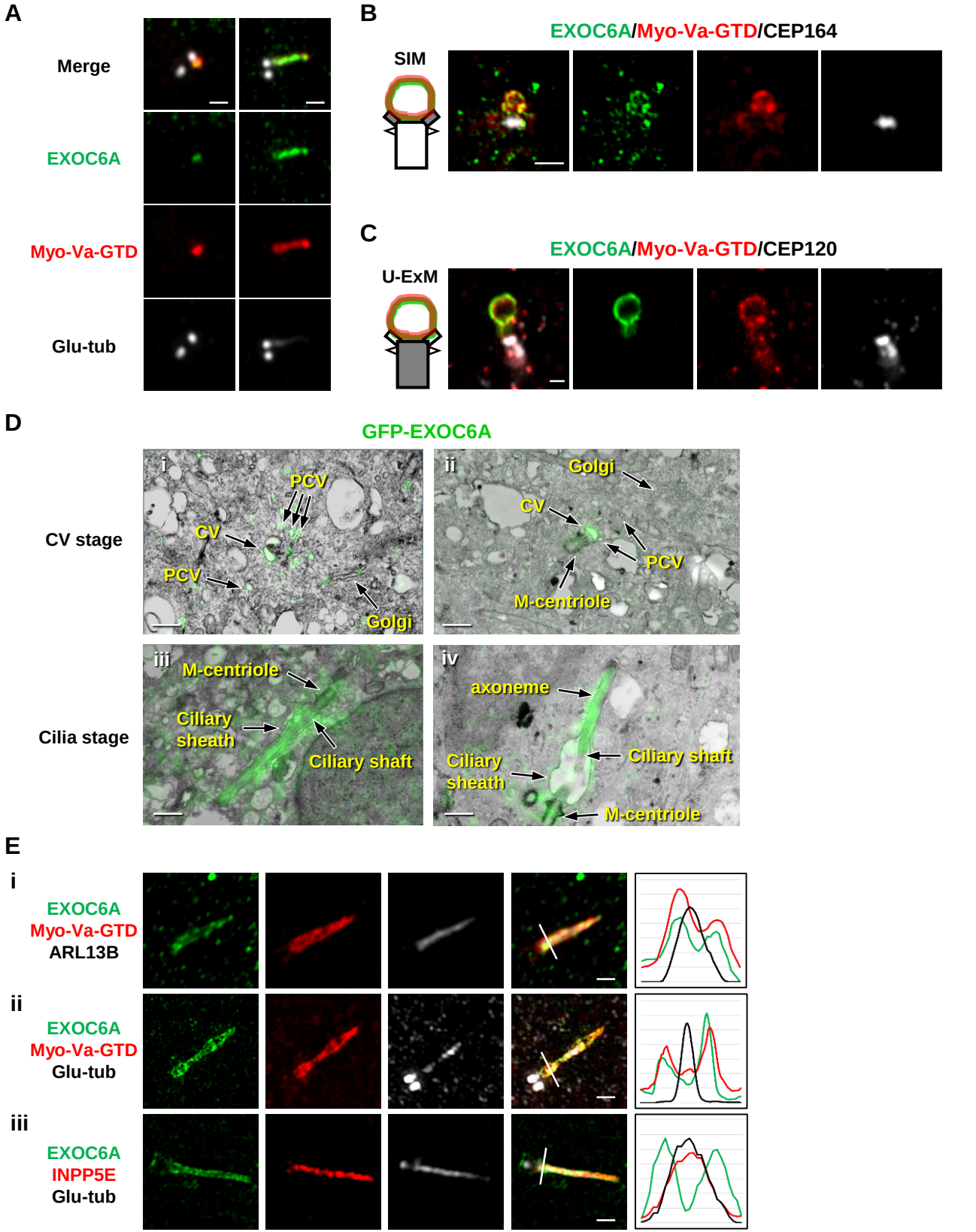
A
Merge
EXOC6A
Myo-Va-GTD
Glu-tub
B
EXOC6A/Myo-Va-GTD/CEP164
SIM
C
EXOC6A/Myo-Va-GTD/CEP120
U-ExM
D
GFP-EXOC6A
CV stage
i
PCV
CV
PCV
Golgi
ii
Golgi
CV
PCV
M-centriole
Cilia stage
iii
M-centriole
Ciliary sheath
Ciliary shaft
iv
axoneme
Ciliary sheath
Ciliary shaft
M-centriole
E
i
EXOC6A
Myo-Va-GTD
ARL13B
ii
EXOC6A
Myo-Va-GTD
Glu-tub
iii
EXOC6A
INPP5E
Glu-tub

Figure. 2

A

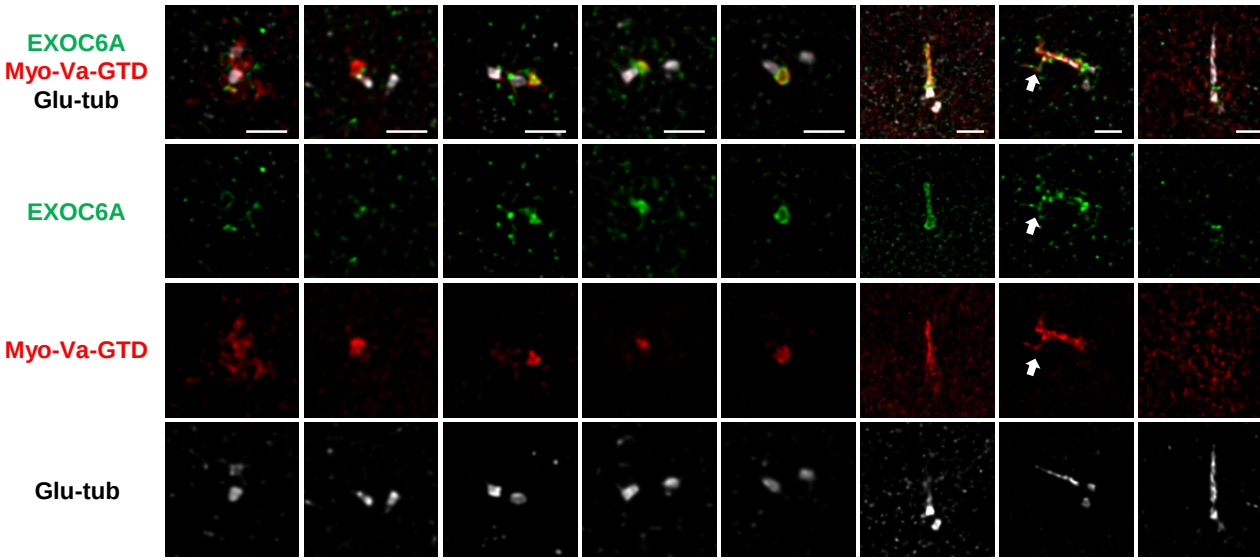

0min	15min	30min	45min	1h	2h	4h	24h
Type 1	Type 2	Type 3			Type 4		Type 5
		EXOC6A^{+}/Va^{+} at CV			EXOC6A^{+}/Va^{+} Elongated cilia		EXOC6A^{-}/Va^{-} Elongated cilia

B

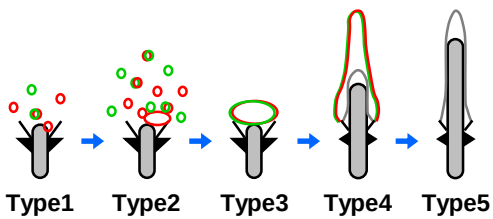

C

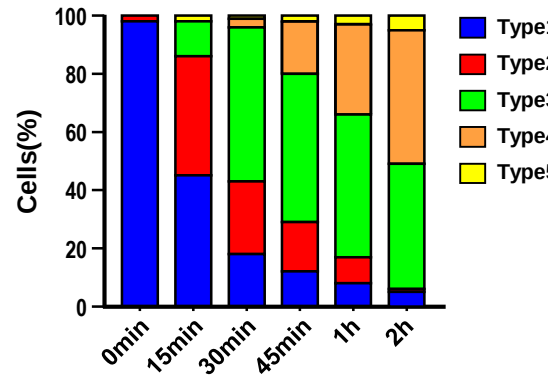

Figure. 3

A

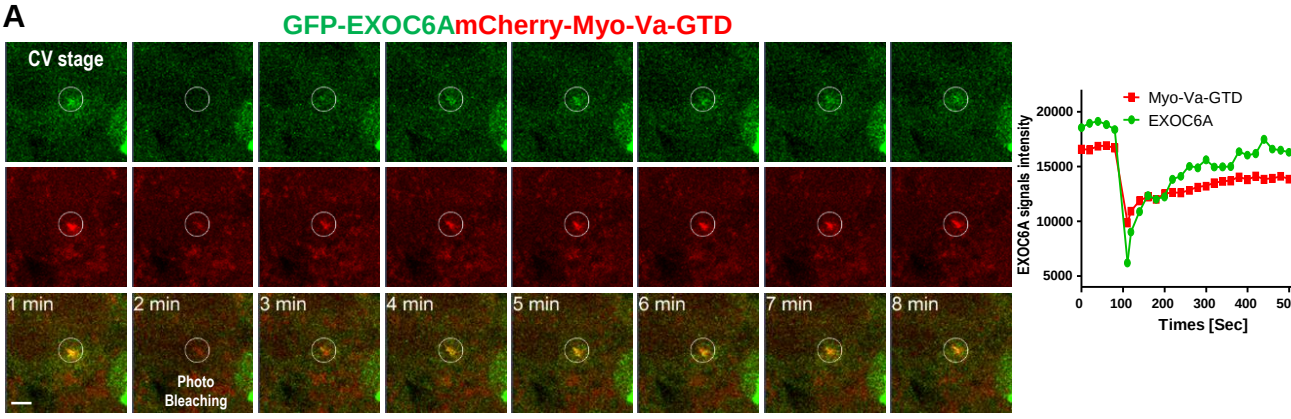

B

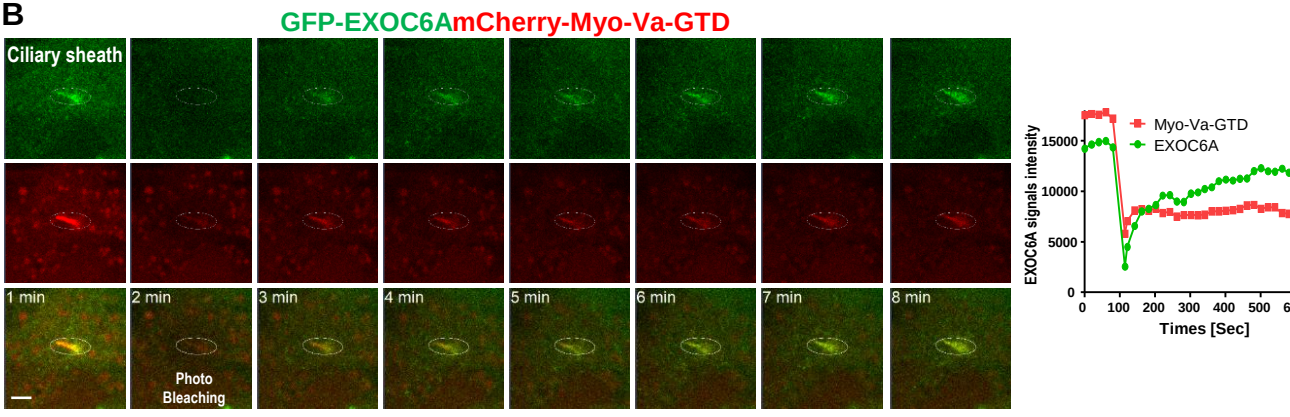

C

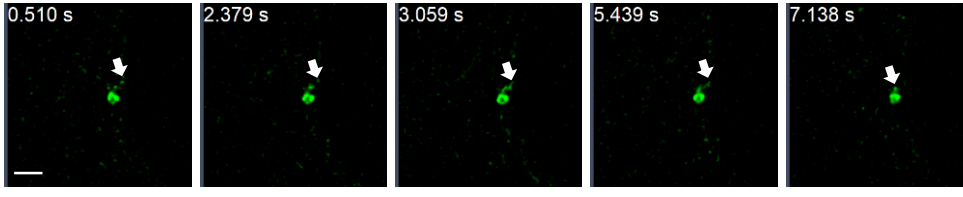

D

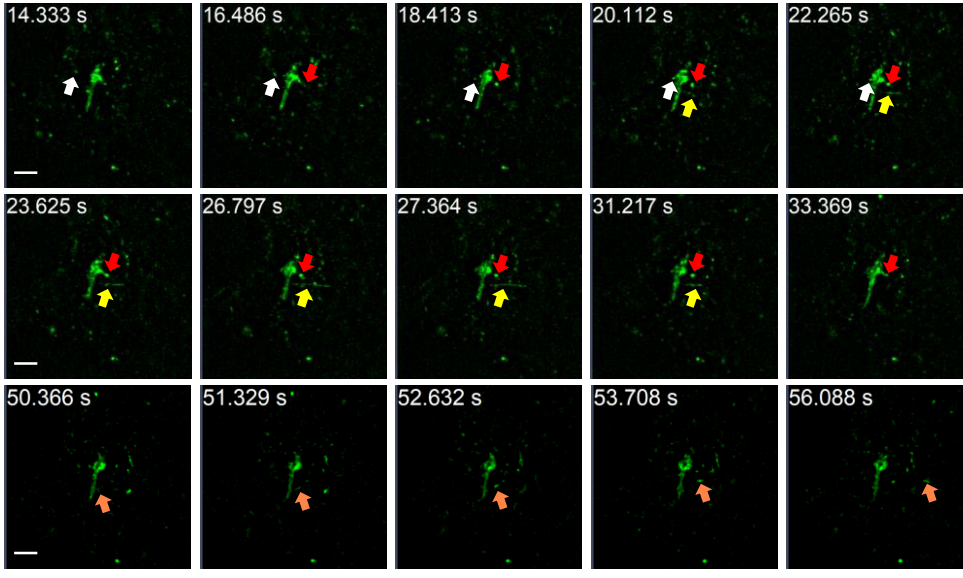

Figure. 4

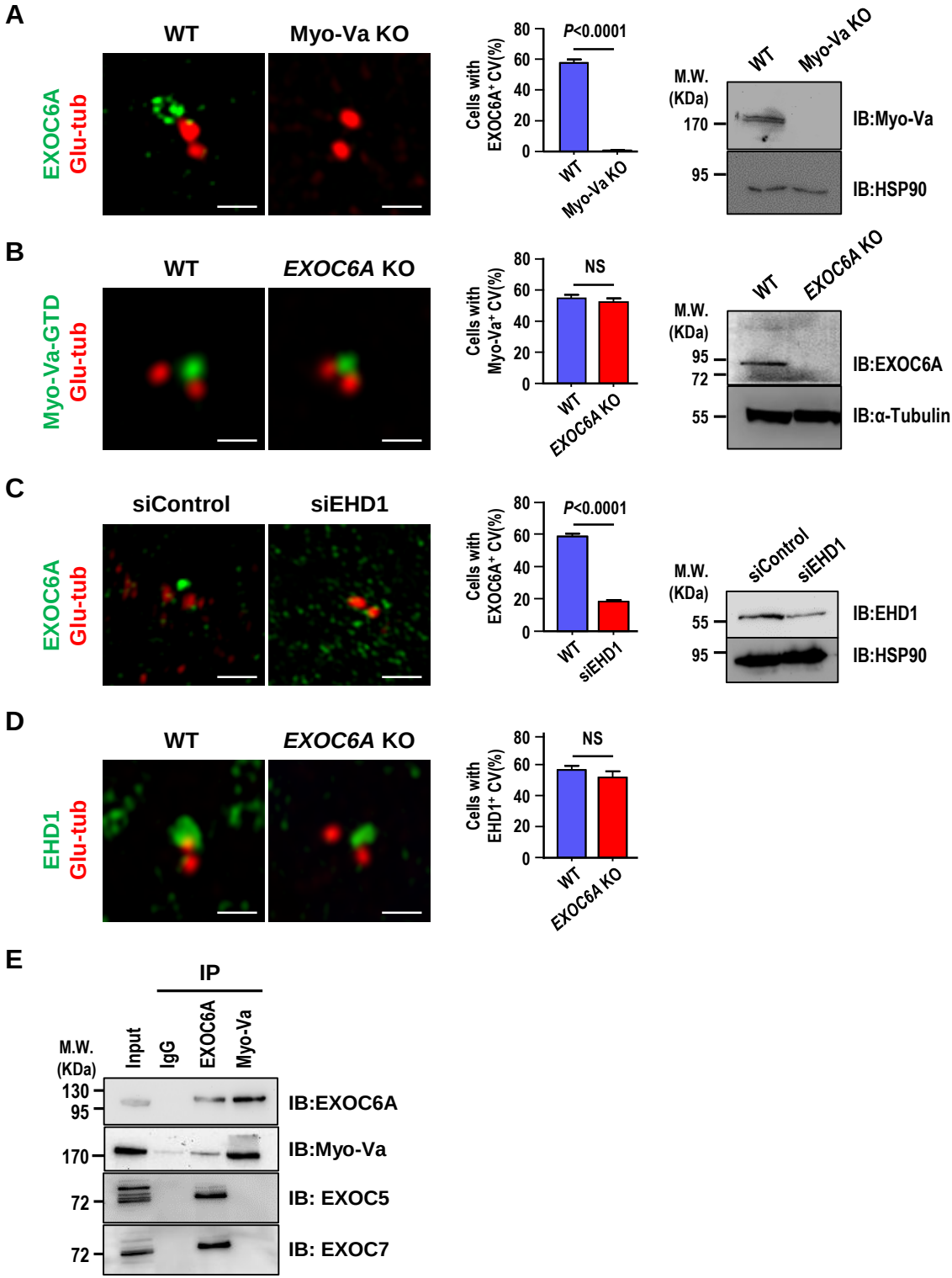
A
WT
Myo-Va KO
EXOC6A
Glu-tub
Cells with EXOC6A+ CV(%)
P<0.0001
WT
Myo-Va KO
M.W. (KDa)
170
95
IB:Myo-Va
IB:HSP90
B
WT
EXOC6A KO
Myo-Va-GTD
Glu-tub
Cells with Myo-Va+ CV(%)
NS
EXOC6A
IB:EXOC6A
IB:α-Tubulin
72
55
C
siControl
siEHD1
Cells with EXOC6A+ CV(%)
IB:EHD1
D
EHD1
Cells with EHD1+ CV(%)
E
IP
Input
IgG
130
IB: EXOC5
IB: EXOC7

Figure. 5

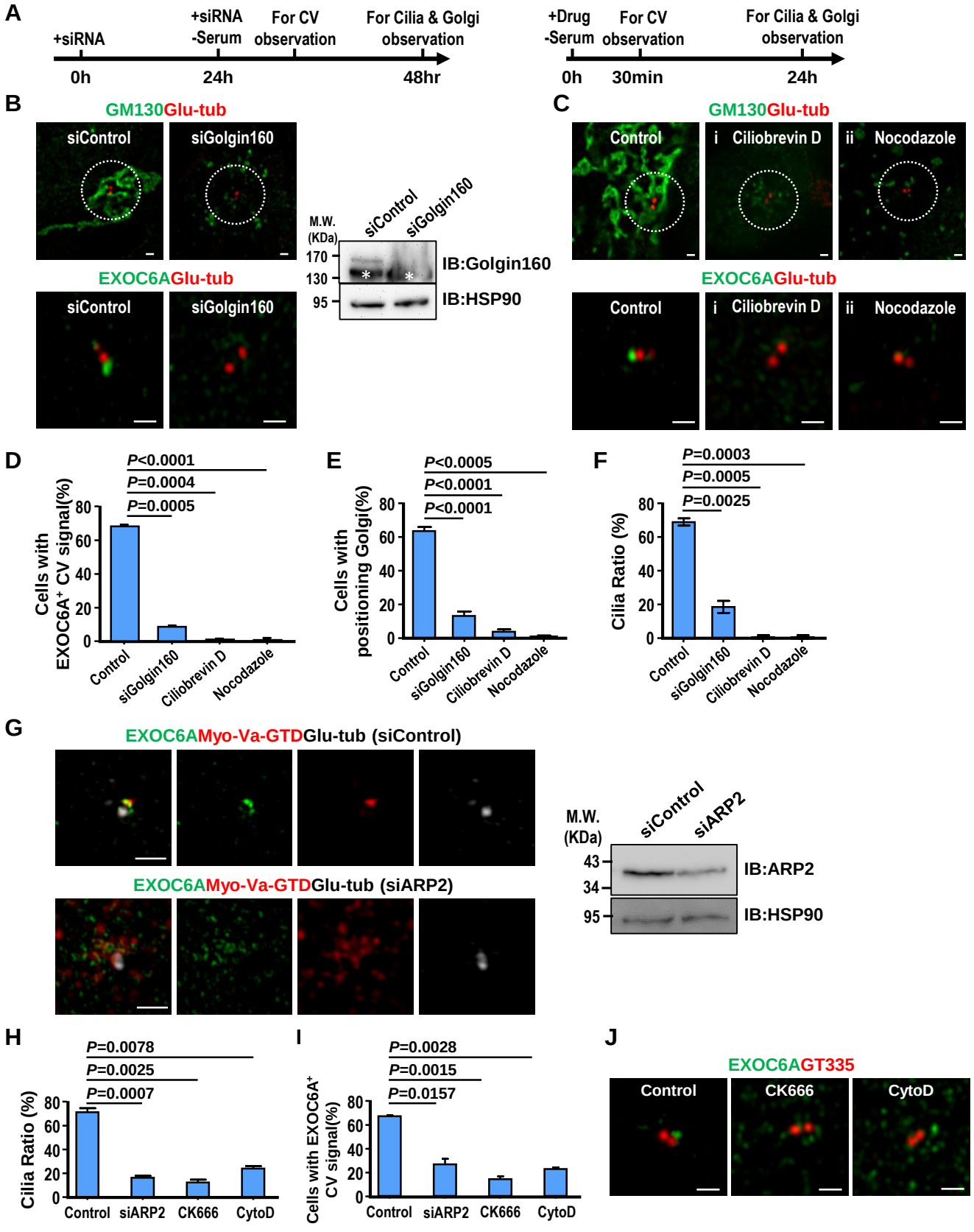
A
+siRNA
+siRNA -Serum
For CV observation
For Cilia & Golgi observation
0h
24h
48hr
+Drug -Serum
For CV observation
For Cilia & Golgi observation
0h
30min
24h
B
GM130Glu-tub
siControl
siGolgin160
EXOC6AGlu-tub
siControl
siGolgin160
M.W. (KDa)
siControl
siGolgin160
170
130
95
IB:Golgin160
IB:HSP90
C
GM130Glu-tub
Control
i Ciliobrevin D
ii Nocodazole
EXOC6AGlu-tub
Control
i Ciliobrevin D
ii Nocodazole
D
P<0.0001
P=0.0004
P=0.0005
Cells with EXOC6A+ CV signal(%)
Control
siGolgin160
Ciliobrevin D
Nocodazole
E
P<0.0005
P<0.0001
P<0.0001
Cells with positioning Golgi(%)
Control
siGolgin160
Ciliobrevin D
Nocodazole
F
P=0.0003
P=0.0005
P=0.0025
Cilia Ratio (%)
Control
siGolgin160
Ciliobrevin D
Nocodazole
G
EXOC6AMyo-Va-GTDGlu-tub (siControl)
EXOC6AMyo-Va-GTDGlu-tub (siARP2)
M.W. (KDa)
siControl
siARP2
43
34
95
IB:ARP2
IB:HSP90
H
P=0.0078
P=0.0025
P=0.0007
Cilia Ratio (%)
Control
siARP2
CK666
CytoD
I
P=0.0028
P=0.0015
P=0.0157
Cells with EXOC6A+ CV signal(%)
Control
siARP2
CK666
CytoD
J
EXOC6AGT335
Control
CK666
CytoD

Figure. 6

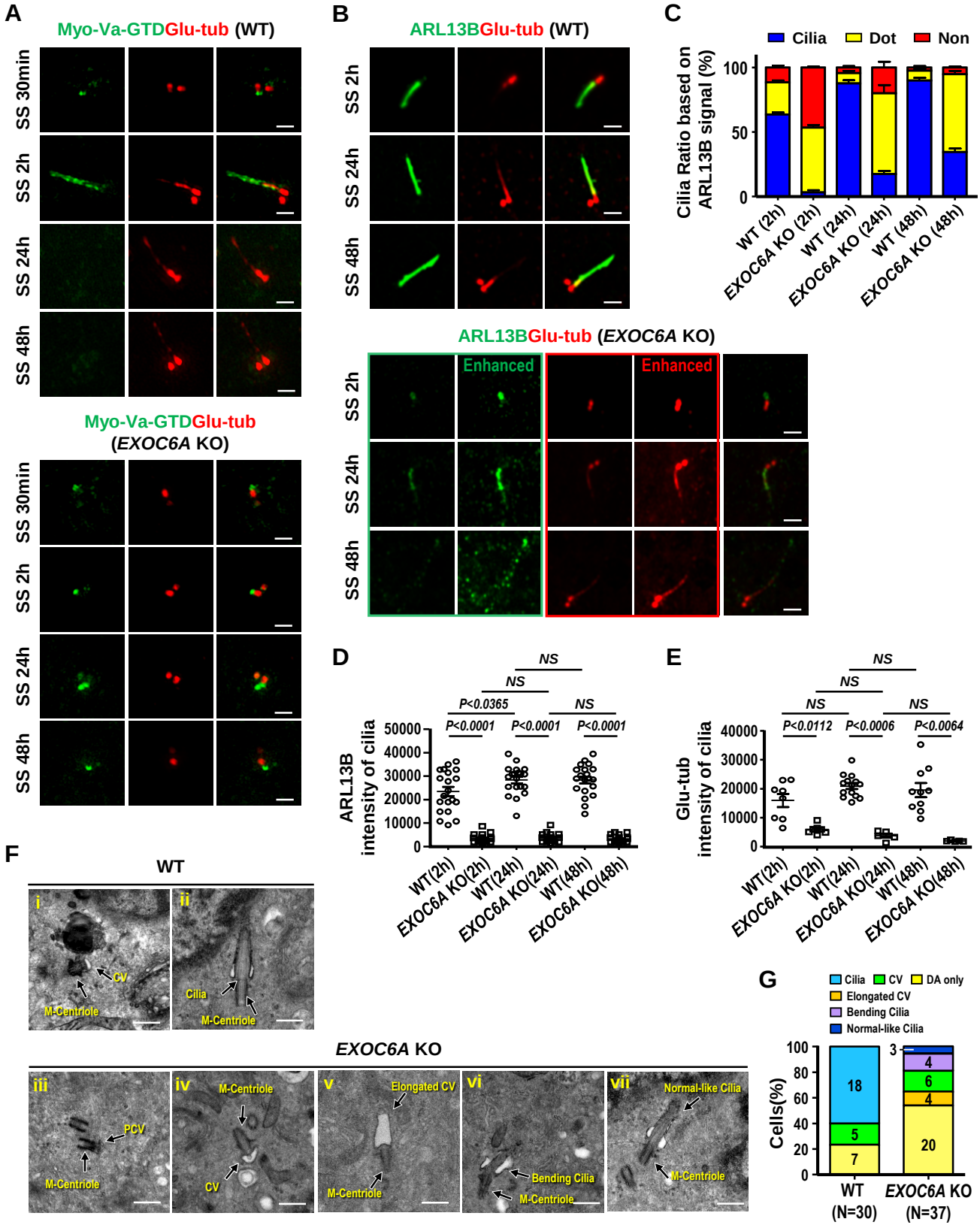
A
Myo-Va-GTDGlu-tub (WT)
SS 30min
SS 2h
SS 24h
SS 48h
Myo-Va-GTDGlu-tub
(EXOC6A KO)
SS 30min
SS 2h
SS 24h
SS 48h
B
ARL13BGlu-tub (WT)
SS 2h
SS 24h
SS 48h
ARL13BGlu-tub (EXOC6A KO)
Enhanced
Enhanced
SS 2h
SS 24h
SS 48h
C
Cilia
Dot
Non
Cilia Ratio based on ARL13B signal (%)
100
50
0
WT (2h)
EXOC6A KO (2h)
WT (24h)
EXOC6A KO (24h)
WT (48h)
EXOC6A KO (48h)
D
ARL13B intensity of cilia
50000
40000
30000
20000
10000
0
NS
NS
P<0.0365
NS
P<0.0001
P<0.0001
P<0.0001
WT(2h)
EXOC6A KO(2h)
WT(24h)
EXOC6A KO(24h)
WT(48h)
EXOC6A KO(48h)
E
Glu-tub intensity of cilia
40000
30000
20000
10000
0
NS
NS
NS
NS
P<0.0112
P<0.0006
P<0.0064
WT(2h)
EXOC6A KO(2h)
WT(24h)
EXOC6A KO(24h)
WT(48h)
EXOC6A KO(48h)
F
WT
i
CV
M-Centriole
ii
Cilia
M-Centriole
EXOC6A KO
iii
PCV
M-Centriole
iv
M-Centriole
CV
v
Elongated CV
M-Centriole
vi
Bending Cilia
M-Centriole
vii
Normal-like Cilia
M-Centriole
G
Cilia
CV
DA only
Elongated CV
Bending Cilia
Normal-like Cilia
Cells(%)
100
80
60
40
20
0
18
5
7
3
4
6
4
20
WT
(N=30)
EXOC6A KO
(N=37)

Figure. 7

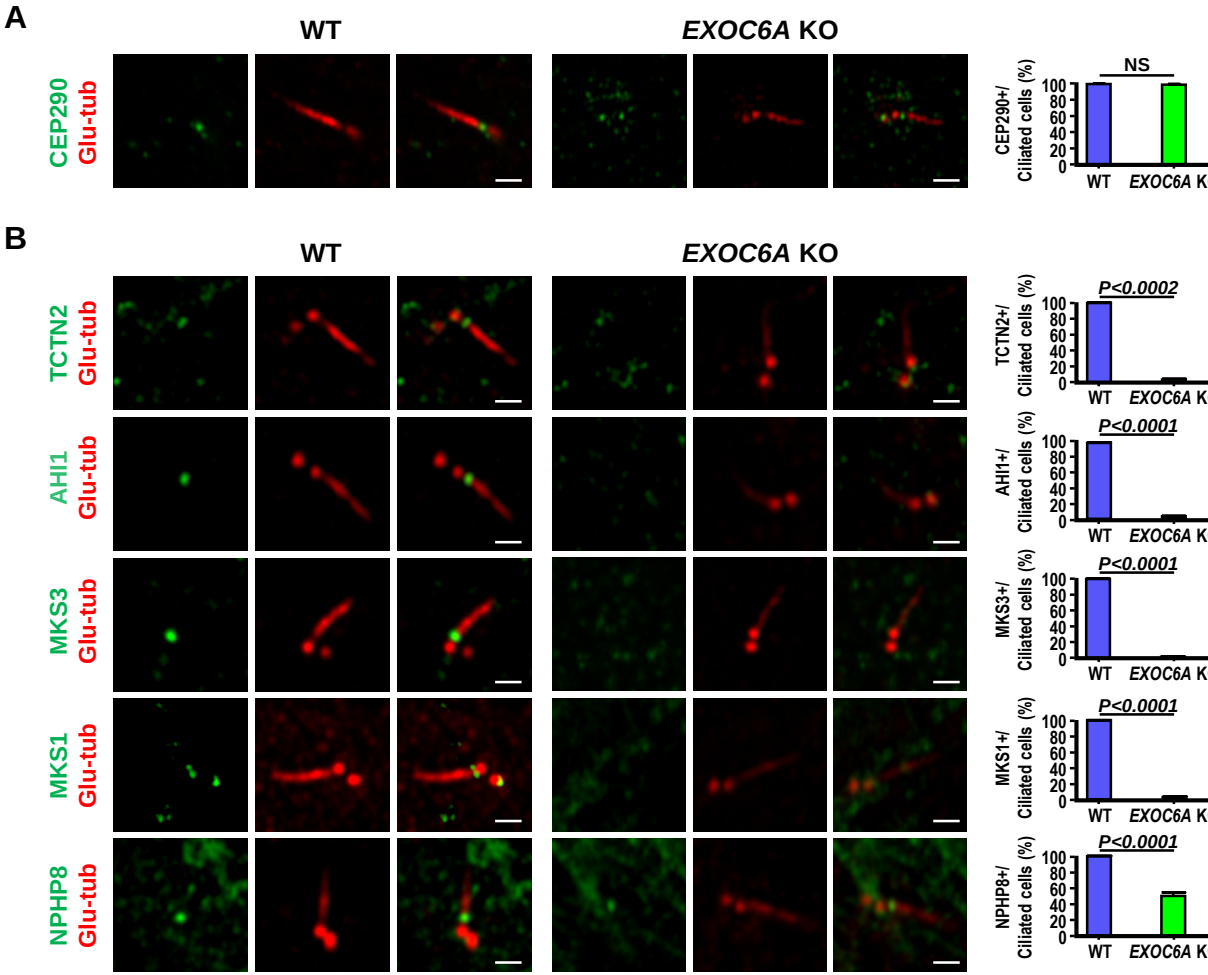
A
WT
EXOC6A KO
CEP290
Glu-tub
CEP290+/ Ciliated cells (%)
NS
100
80
60
40
20
0
WT
EXOC6A KO
B
WT
EXOC6A KO
TCTN2
Glu-tub
TCTN2+/ Ciliated cells (%)
P<0.0002
AHI1
Glu-tub
AHI1+/ Ciliated cells (%)
P<0.0001
MKS3
Glu-tub
MKS3+/ Ciliated cells (%)
P<0.0001
MKS1
Glu-tub
MKS1+/ Ciliated cells (%)
P<0.0001
NPHP8
Glu-tub
NPHP8+/ Ciliated cells (%)
P<0.0001

Figure. 8

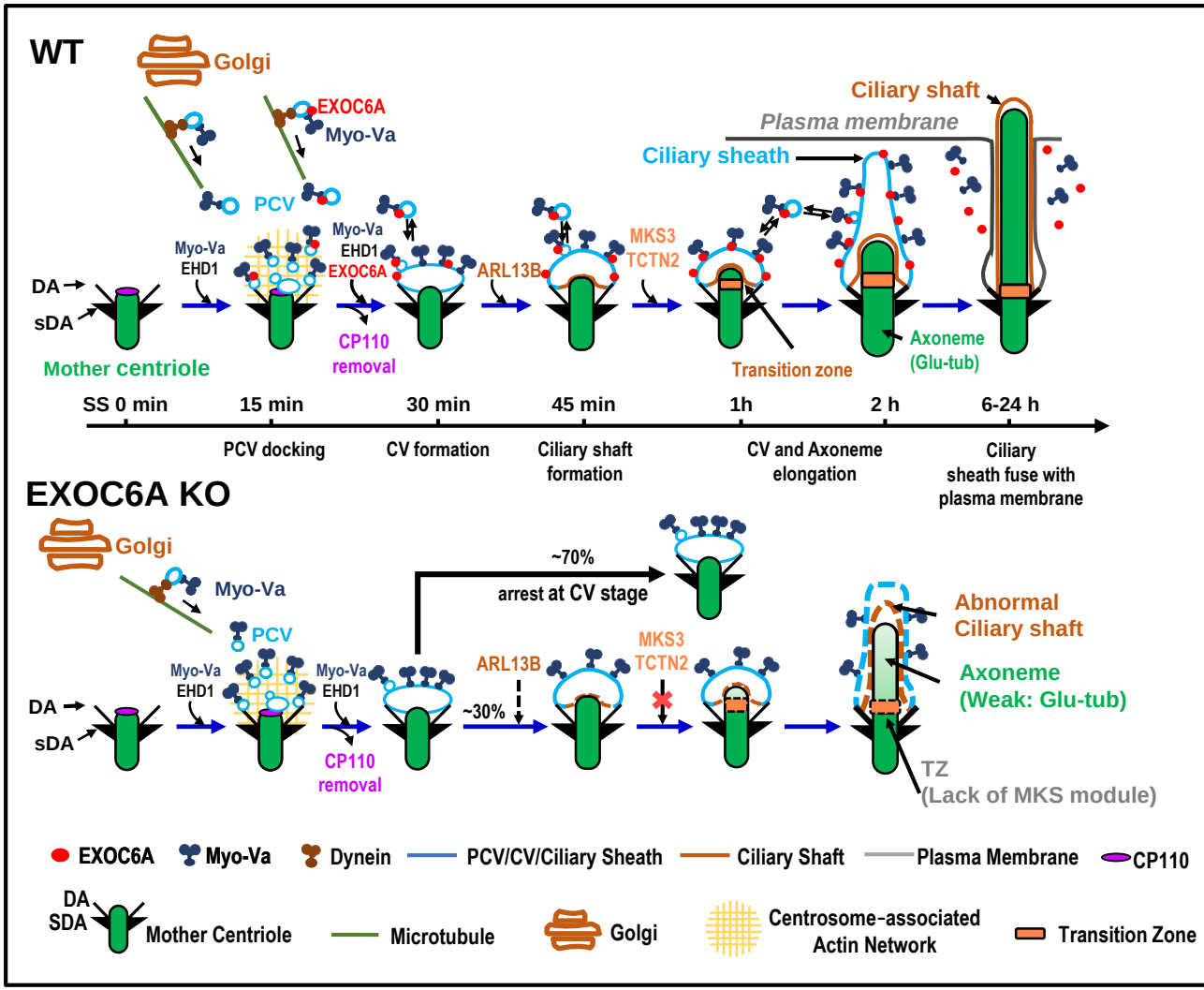
WT
Golgi
EXOC6A
Myo-Va
PCV
Ciliary shaft
Plasma membrane
Ciliary sheath
Myo-Va
EHD1
Myo-Va
EHD1
EXOC6A
ARL13B
MKS3
TCTN2
DA
sDA
Mother centriole
CP110
removal
Transition zone
Axoneme
(Glu-tub)
SS 0 min
15 min
30 min
45 min
1h
2 h
6-24 h
PCV docking
CV formation
Ciliary shaft
formation
CV and Axoneme
elongation
Ciliary
sheath fuse with
plasma membrane
EXOC6A KO
Golgi
Myo-Va
PCV
~70%
arrest at CV stage
Abnormal
Ciliary shaft
Axoneme
(Weak: Glu-tub)
Myo-Va
EHD1
Myo-Va
EHD1
ARL13B
~30%
MKS3
TCTN2
DA
sDA
CP110
removal
TZ
(Lack of MKS module)
EXOC6A
Myo-Va
Dynein
PCV/CV/Ciliary Sheath
Ciliary Shaft
Plasma Membrane
CP110
DA
SDA
Mother Centriole
Microtubule
Golgi
Centrosome-associated
Actin Network
Transition Zone

Supplementary Figure 1

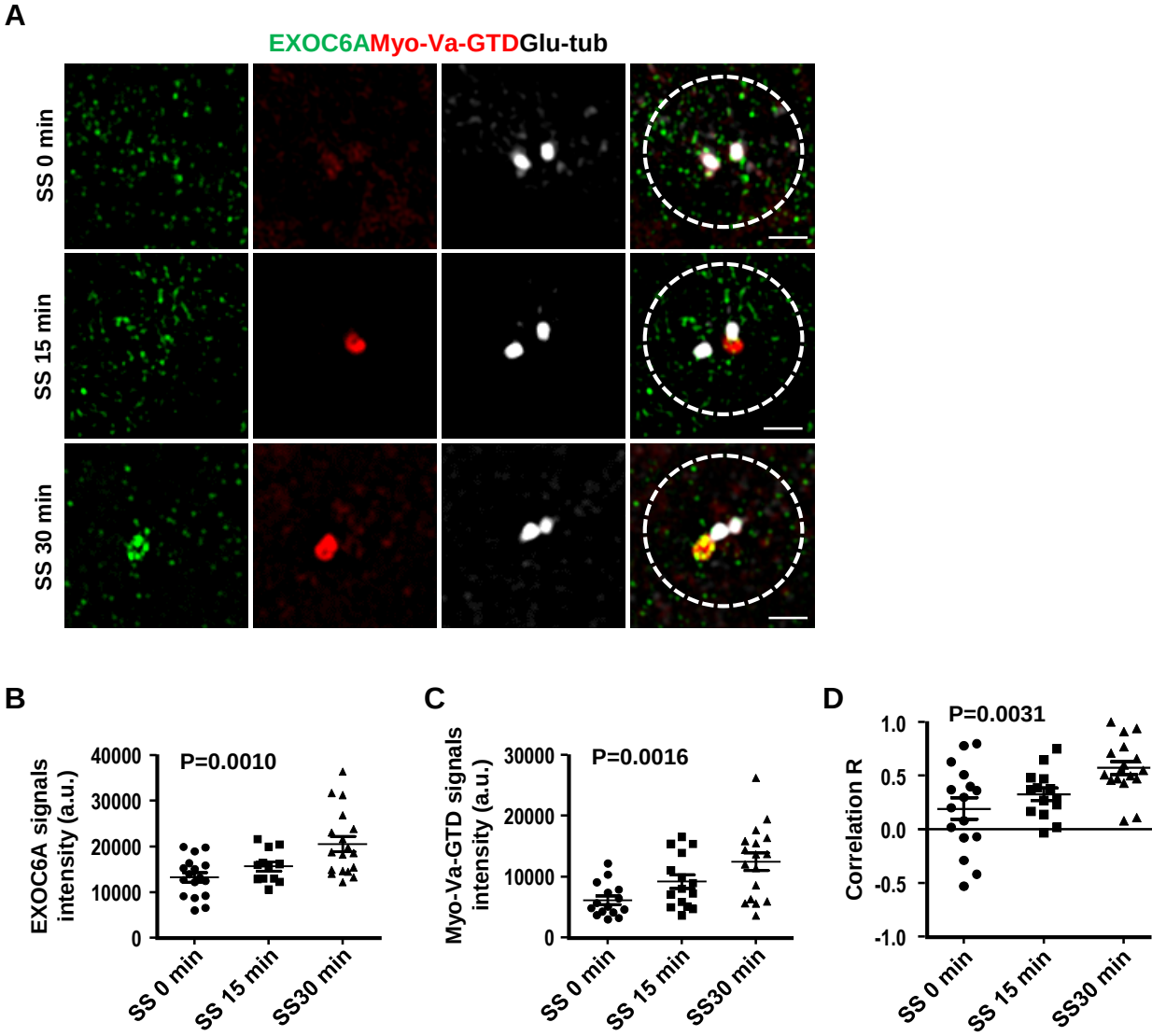

Supplementary Figure 2

A

GFP-EXOC6AmCherry-MyoVa-GTDSir-tubulin

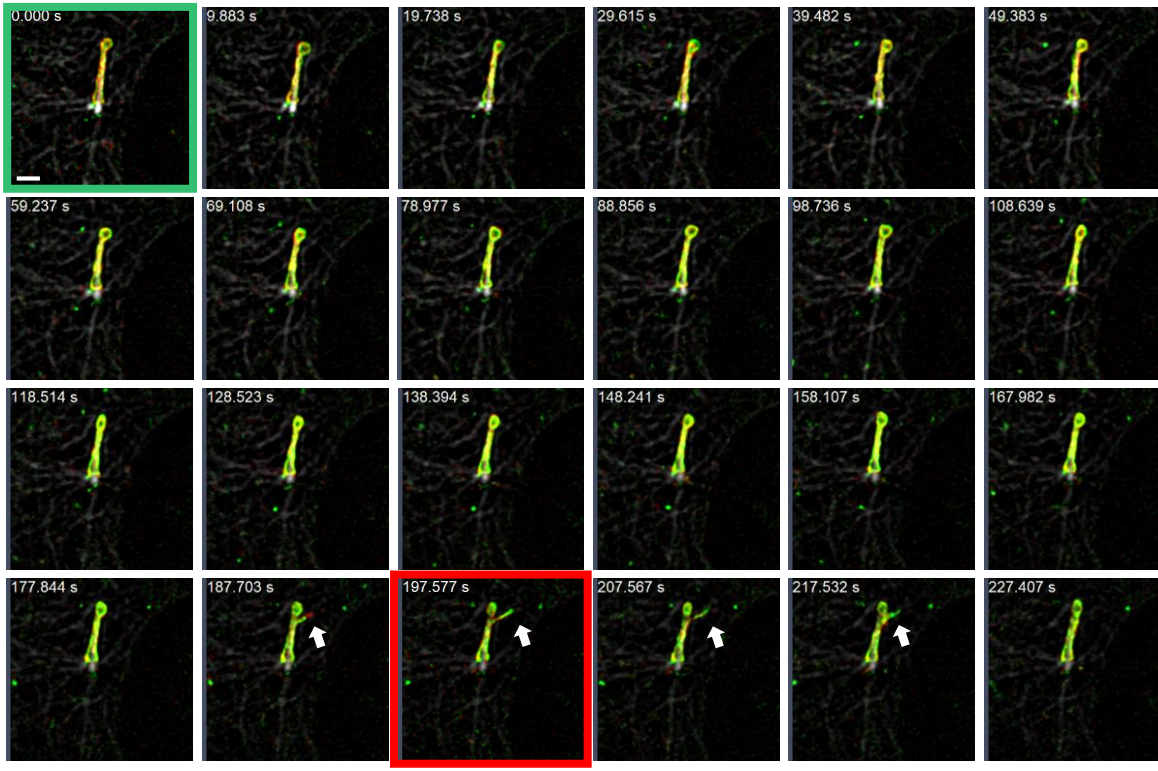

B

GFP-EXOC6AmCherry-MyoVa-GTDSir-tubulin

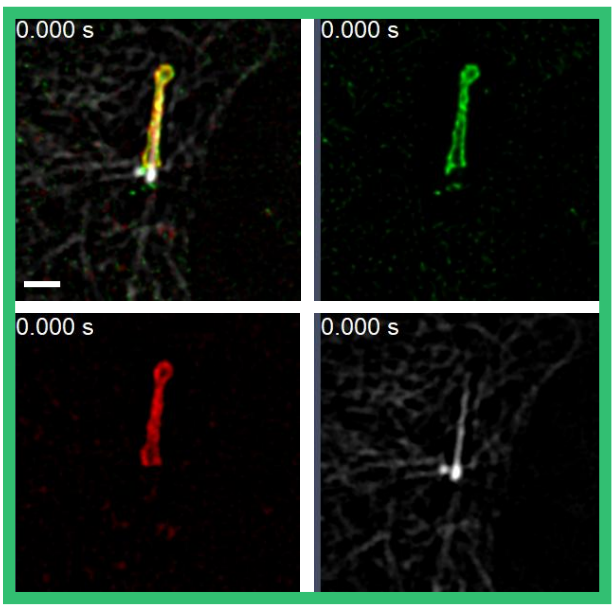

C

GFP-EXOC6AmCherry-MyoVa-GTDSir-tubulin

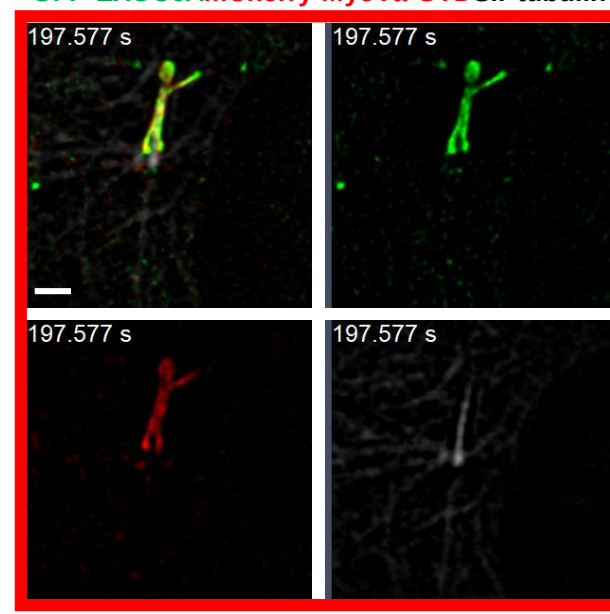

Supplementary Figure 3

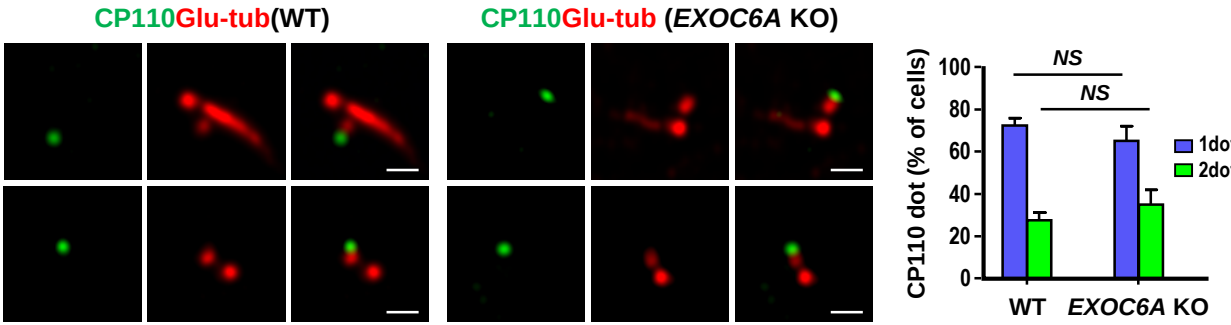

Supplementary Figure 4

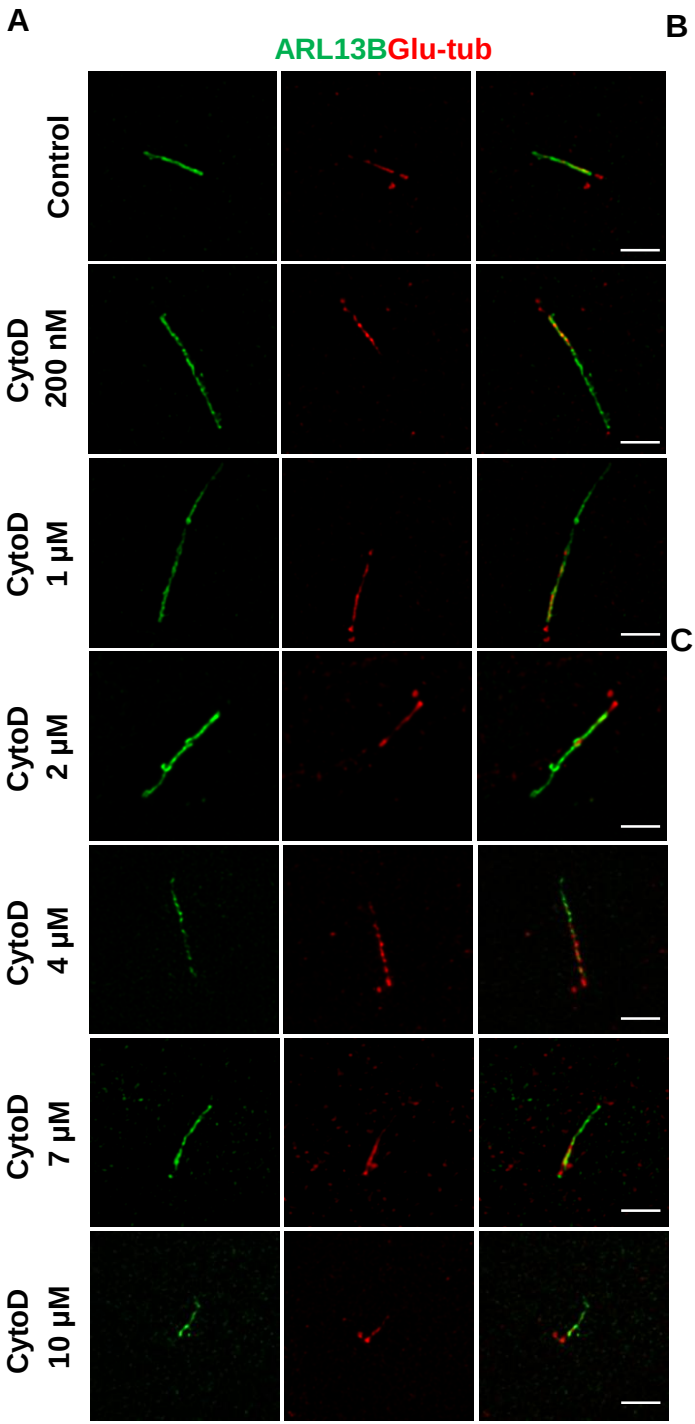

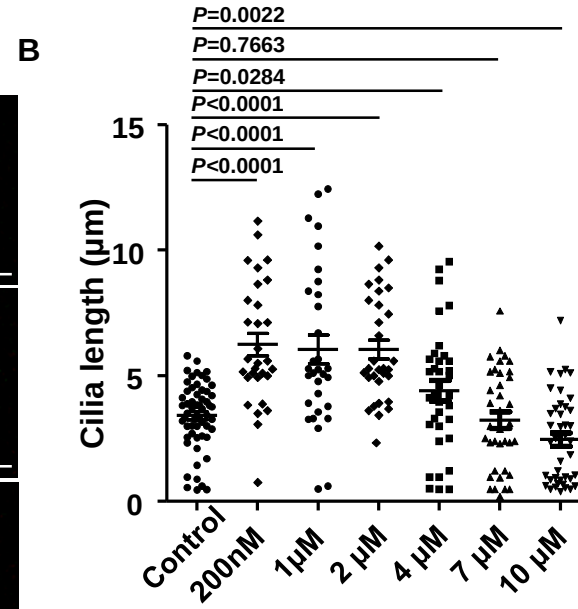

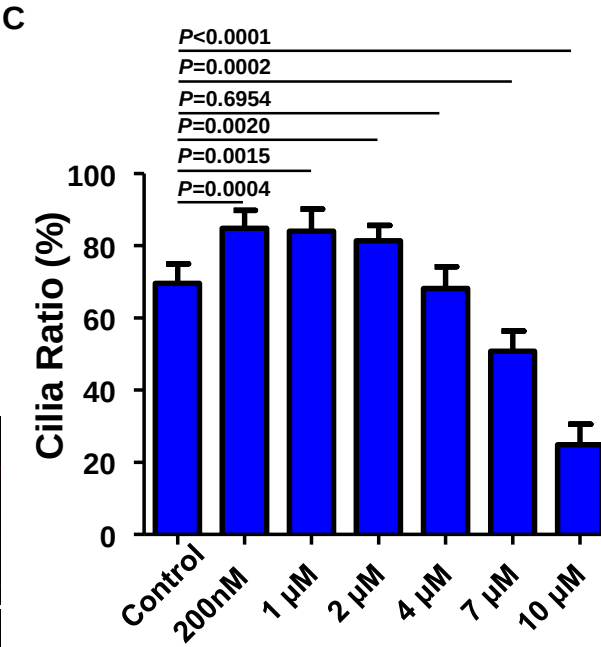

Supplementary Figure 5

A

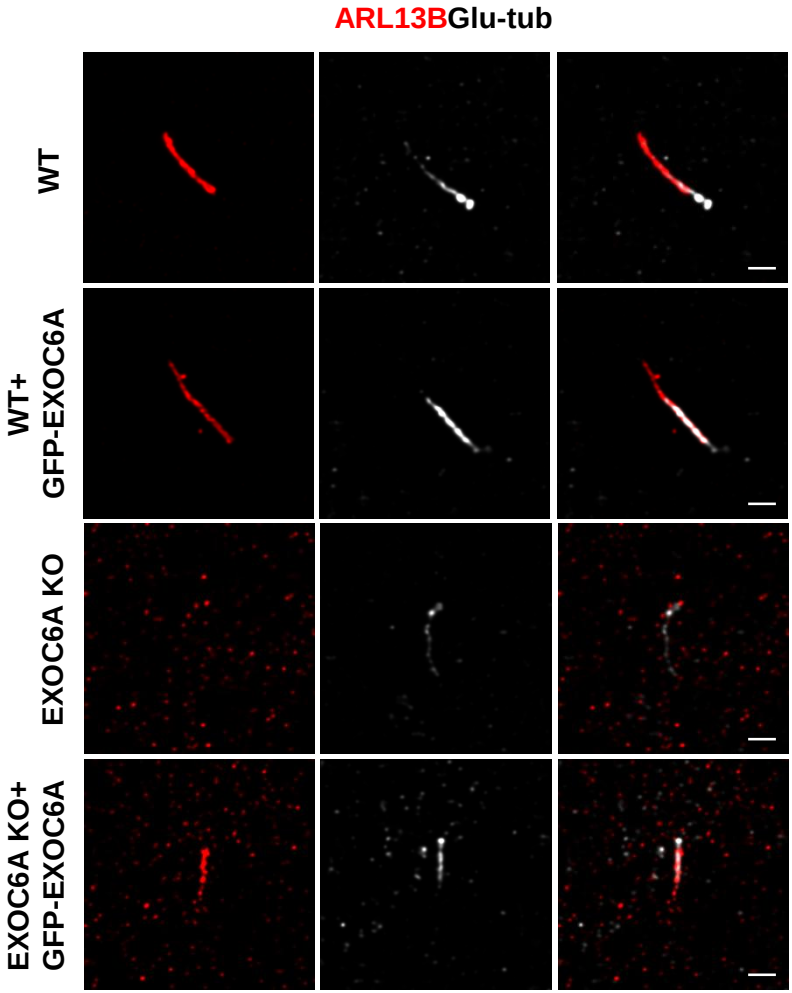

B

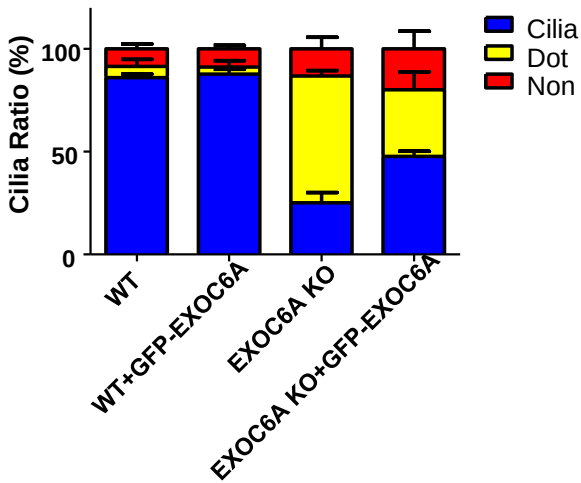

Source Data

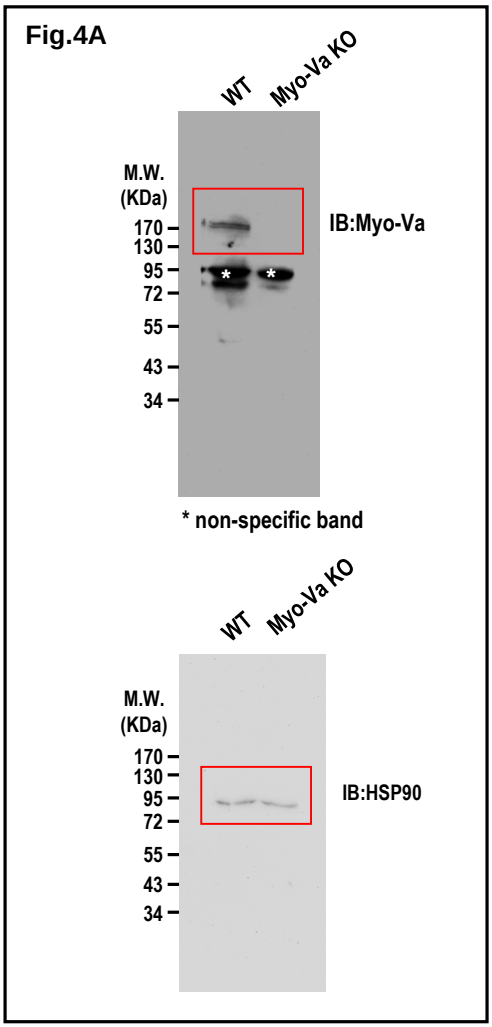
Fig.4A
WT
Myo-Va KO
M.W.
(KDa)
170
130
95
72
55
43
34
IB:Myo-Va
* non-specific band
WT
Myo-Va KO
M.W.
(KDa)
170
130
95
72
55
43
34
IB:HSP90

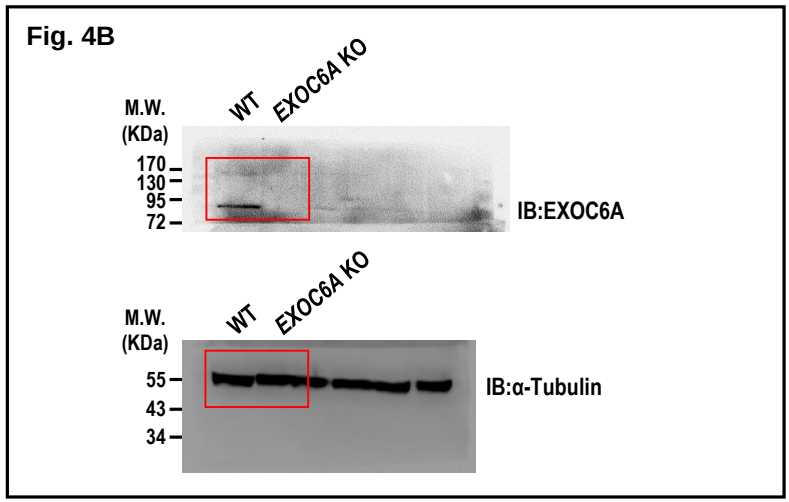
Fig. 4B
M.W.
(KDa)
WT
EXOC6A KO
170
130
95
72
IB:EXOC6A
M.W.
(KDa)
WT
EXOC6A KO
55
43
34
IB:α-Tubulin

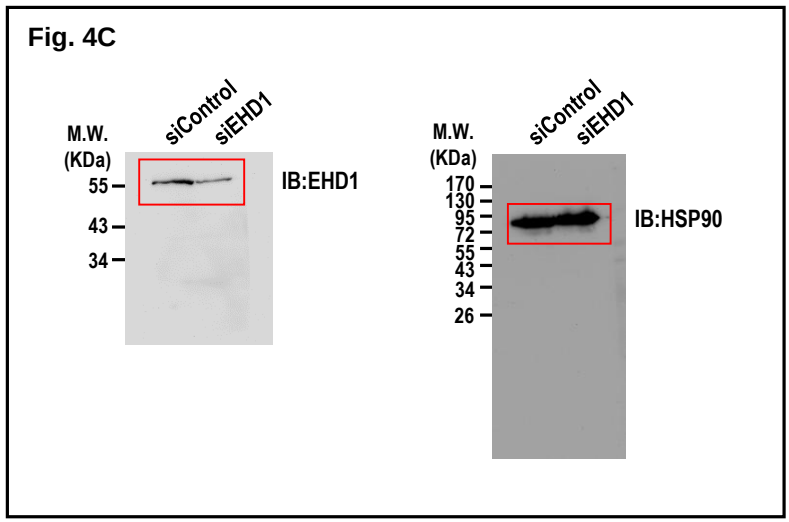
Fig. 4C
M.W.
(KDa)
siControl
siEHD1
55
43
34
IB:EHD1
M.W.
(KDa)
siControl
siEHD1
170
130
95
72
55
43
34
26
IB:HSP90

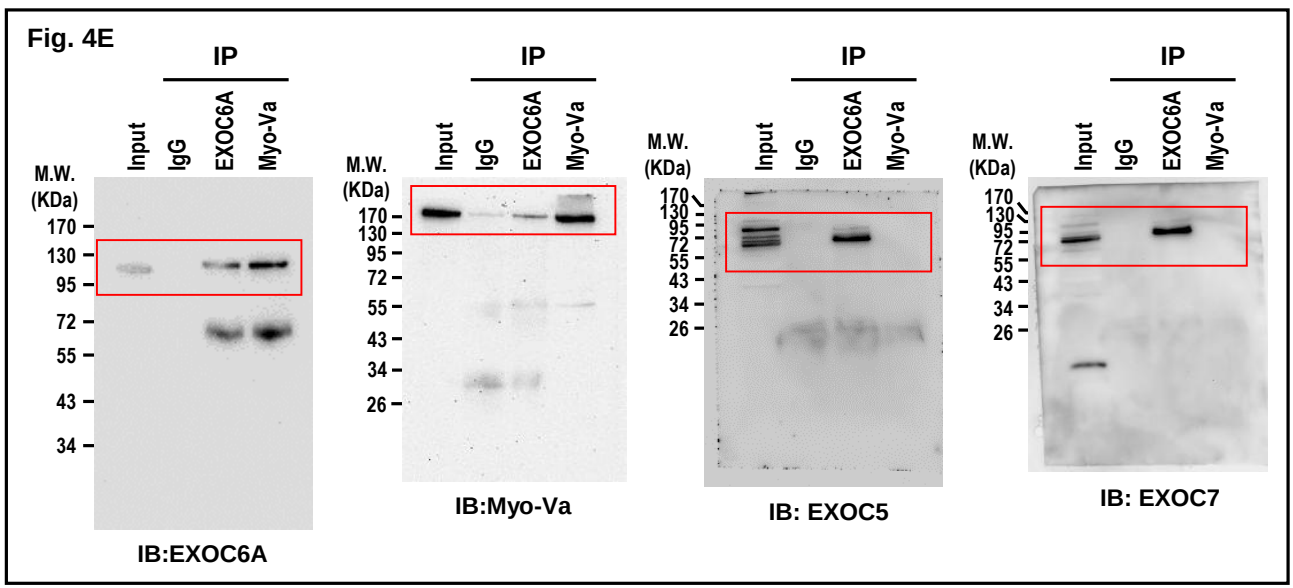
Fig. 4E
IP
Input
IgG
EXOC6A
Myo-Va
M.W.
(KDa)
170
130
95
72
55
43
34
IB:EXOC6A
IP
Input
IgG
EXOC6A
Myo-Va
M.W.
(KDa)
170
130
95
72
55
43
34
26
IB:Myo-Va
IP
Input
IgG
EXOC6A
Myo-Va
M.W.
(KDa)
170
130
95
72
55
43
34
26
IB: EXOC5
IP
Input
IgG
EXOC6A
Myo-Va
M.W.
(KDa)
170
130
95
72
55
43
34
26
IB: EXOC7

Source Data

Fig. 5B

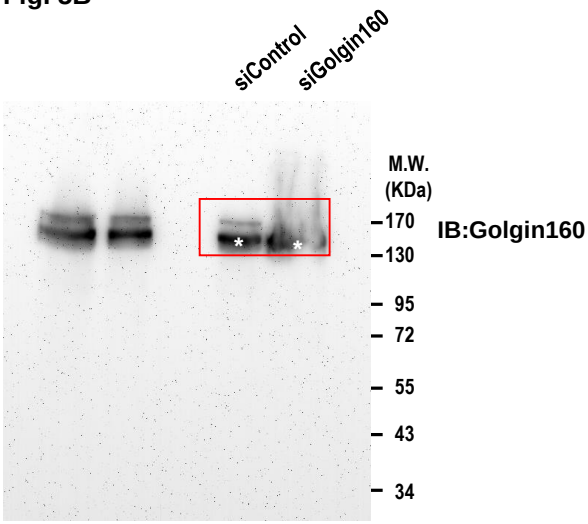

* non-specific band

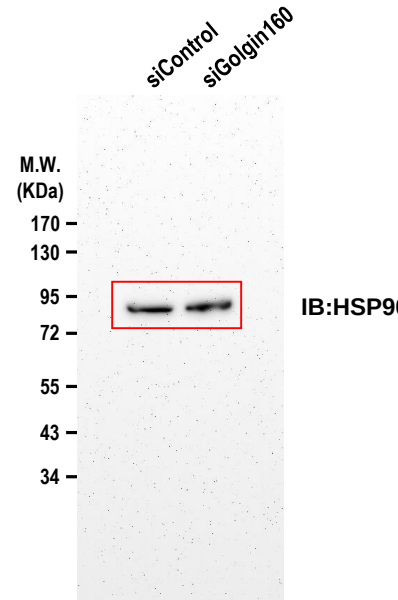
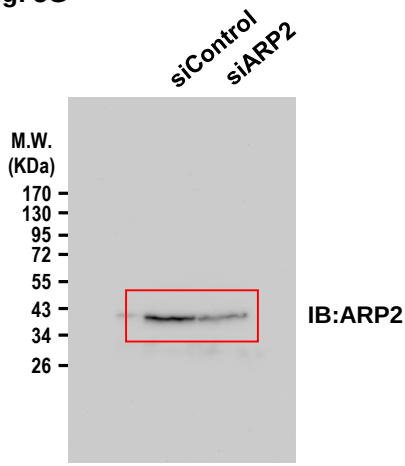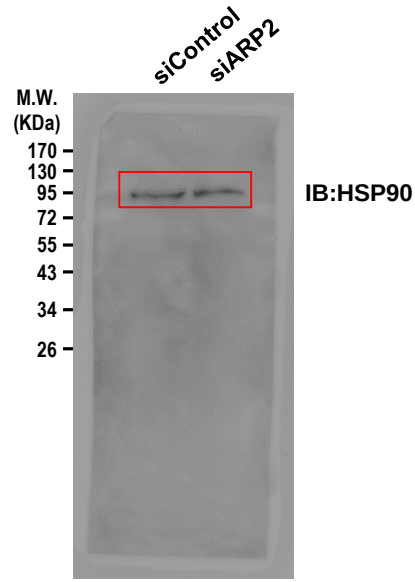
Fig. 5G